LAWRENCE
LIVERMORE
NATIONAL
LABORATORY

UCRL-JRNL-222027

Up-Dating Of Atomic Data Needed For Ionisation Balance Evaluations of Krypton and Molybdenum

M. Mattioli, G. Mazzitelli, K. B. Fournier, M. Finkenthal, L. Carraro

June 13, 2006

Journal of Physics B: Atomic, Molecular and Optical Physics

Up-dating of atomic data needed for ionisation balance evaluations of Krypton and Molybdenum

M. Mattioli [a] , G. Mazzitelli [b], K.B. Fournier [c], M. Finkenthal [d], L. Carraro [a]

a Consorzio RFX, Associazione Euratom-Enea sulla Fusione, Corso Stati Uniti 4, Padova, I-35127, Italy
b Associazione Euratom-Enea sulla Fusione, C. R. Frascati, CP 65-00044, Frascati Roma Italy
c Lawrence Livermore National Laboratory, PO Box 808, L-41 Livermore, CA 94550, USA
d Department of Physics and Astronomy, the Johns Hopkins University, Baltimore, MD 21218 USA

Abstract

Atomic data for both ionisation and recombination of Kr and Mo ions are reviewed, since the rate coefficients for these processes need to be regularly up-dated following the publication of new theoretical calculations and new experimental data. Kr is used in magnetic-confinement-fusion devices to produce a peripheral radiating mantle meant to spread the heat load on the plasma-facing components. In a few tokamaks Mo tiles cover the plasma-facing surfaces, acting in most cases as a plasma-column limiter. The collected atomic data represent the state of the art on the ionisation and recombination data for the two considered elements. Samples of rates are proposed for both ionisation and recombination along with tables of the fractional abundances at ionisation equilibrium. The proposed rates should be included in codes that simulate the impurity behaviour in magnetic-confinement-fusion devices, i.e., when radial transport is added to ionisation and recombination to predict spatially resolved charge-state distributions that are to be compared with experimental results.

1. Introduction

For the interpretation of experimental data from both astrophysical sources and magnetic confinement fusion (MCF) devices atomic data for both ionisation and recombination are required. The rates for these processes have to be regularly up-dated following the publication of new theoretical calculations and new experimental data. Astrophysicists usually consider only elements up to Cu (Z=29) or Zn (Z=30). An article that updates recommended data from recent references is published every five or six years allowing determination of charge state distributions (CSD) at ionisation equilibrium. At present, the most recent article in this context is the 1998 paper from Mazzotta et al. [1], which has been extended in Ref. [2] from Cu to Ge (Z=32). Since experimental data from both Kr (Z=36) and Mo (Z=42) are available from MCF

devices, atomic data are also needed for these two elements. Their radiation-loss patterns were considered first by Post et al. [3, 4] and, more recently, by Fournier et al. [5, 6].

Inert gases (Ne, Ar, Kr) can be added in MCF devices to the fuelling gas to produce a peripheral radiating mantle which spreads the heat load on the plasma-facing components. Interest in these inert-gas scenarios has been increased by the fact that improved-confinement and high-density regimes (called radiatively improved [RI] modes) have been obtained both on limiter and divertor tokamaks like JET, DIII-D and TEXTOR [7-10]. On the other hand, in the Alcator C-Mod and FTU devices Mo tiles cover the plasma-facing surfaces, acting in most cases as a plasma-column limiter. For Kr, May et al. [11] experimentally obtained Kr ion density profiles and the associated cooling rates on FTU, which were tested against the model proposed by Fournier et al in Ref. [5]. For Mo, both on Alcator C-Mod and on FTU similar comparisons are reported in Ref. [12] with calculated radiative losses in Ref. [6]. On TEXTOR Mo accumulation has been reported both with a test Mo limiter [13] and in presence of Ne edge radiation cooling [10]. Between the other published papers focused on the Mo ion distribution one should mention Refs. [14, 15] and Ref. [16], respectively, for Alcator C-Mod and FTU. At the present an open question is the Mo ion CSD, when the central electron temperature T_e is larger than about 4 keV, i.e., when the most abundant ions range from F-like to Li-like. On FTU Pacella et al. [17] analysed with moderate spectral resolution the 0.5 - 5.5 Å spectral range for a plasma heated to ~7 – 8 keV by electron-cyclotron-resonance heating. The Mo spectrum (due to $\Delta n=1$ 3-2 transitions) could be simulated with the central plasma near coronal equilibrium and with impurity peaking. On the other hand, Mattioli et al. [18] analysed Mo spectra from the JET tokamak in the 35 - 60 Å spectral range, where the Mo lines originate from $\Delta n=0$ 2-2 transitions of F-like to Li-like ions. With the CSD data for Mo quoted in Ref. [16], it was not possible to simulate the JET Mo spectrum obtained by laser blow-off (LBO) injection. It has been necessary to modify the CSD by reducing by a factor of two the ionisation /recombination ratio for F-like to B-like ions. On the other hand, for hot (> 4 keV) FTU plasmas it has not been possible to conclude if the same correction was necessary. Finally, since theory predicts central peaking of impurities in MCF devices increasing in strength with the atomic number Z, comparison of the behaviour of different Z elements is necessary in impurity-transport studies. Examples of such studies (i.e., when different elements are analysed in similar discharges with weak gas seeding and/or with LBO injections) have already been reported on ASDEX Upgrade and on JET [19, 20]. Mo and Kr have been considered, respectively, in Refs [18, 19].

In our previous work on impurity transport for Kr the atomic data came, at least for the highly charges ions, from Ref. [5], whereas for Mo, as already said, the corresponding data have been described in Ref. [16]. Concerning ionisation, Kr ionisation rate coefficients have been obtained recently by Loch et al. for all the 36 ions [21], but the corresponding rate coefficients for the 42 Mo ions are not available at the moment. Experimental ionisation cross sections are available for all ions up to Ar-like Kr XIX (with the exception of Zn-like Kr VII) and up to Se-like Mo IX; these cross-section data are summarized in Section 2. In Section 3, from fits to the cross sections as function of energy, ionisation rate coefficients are evaluated. The difficulty caused by the presence of populated metastable levels (related to the electron density inside the source) in the ion beams extracted from the ion sources where the cross-section data were measured is discussed. We justify the use of experimental data, where available, for the ionisation rates to be used for simulating impurity behaviour in MCF devices. In absence of these data theoretical rates are proposed.

In Section 4 recombination data are assessed. For dielectronic recombination (DR) a coordinated programme has been started under the leadership of Nigel Badnell of the University of Strathclide [22]. In this reference goals and methodology of the modelling of finite-density plasmas are discussed. All the elements up to Zn are included, plus Kr, Mo and Xe. Tables of coefficients from fits of the detailed calculations are proposed. Not only is the T_e range of collisionally ionised plasmas considered (i.e., that of MCF devices), but calculations extend down to the low-T_e, astrophysical photoionised plasma regime. For all the sequences from recombining H–like to Na-like ions (but not yet for the He-like recombining sequence) papers have been published in Astronomy and Astrophysics. Everything is 'centralised' on the University of Strathclyde web site [23], where tables are given for all the sequences from recombining H-like to Na-like ions. On the same web site similar tables for radiative recombination (RR) are available for the same atomic species from recombining, fully stripped to Na-like ions and a regular paper has been submitted [24]. The data from the coordinated programme on DR are taken from the web site, where all the corrections included in the Errata to a few of the published papers can be found. For less-ionised ions, few detailed calculations exist. When these are missing, for DR the general Burgess-Merts (BM) formula is used [25, 26]. For RR, on the other hand, only the simple, coarse approximation of recombination into a partially filled valence band and into H-like excited levels is available (see, e. g., the review article [27]). Its reliability has been checked by comparison with the data of Ref. [24]. Complete tables of fitting coefficients for both ionisation and recombination data are given.

The CSD at ionisation equilibrium is evaluated using the present data, and tables of the ion fractional abundances f_Z, as functions of electron temperature T_e, are given along with concluding remarks in Section 5. We judge that the proposed ionisation and recombination rates represent the state of the art of the available atomic data. The proposed rates should be included in the codes simulating impurity behaviour in MCF devices, i.e., when radial transport is added to ionisation and recombination to predict spatially resolved CSDs that are to be compared with experimental results.

2. Ionisation cross sections

2.1 Krypton ions

Experimental data on ionisation cross sections σ as a function of the impacting-electron energy E are available for the Kr ions from neutral Kr I up to Ar-like Kr XIX, with the single exception of Zn-like Kr VII. These data are given in Refs [28-38] and are individually treated in the following discussion. Supplementary unpublished $\sigma(E)$ data by D. Gregory for Kr VIII and Kr X and by R. Howald for Kr V can be found on the Oak Ridge National Laboratory (ORNL) web site [39]. Recommended data (up-dated in 1998 at the Queen's University, Belfast) for Kr I-IV and theoretical $\sigma(E)$ for Kr I are given, respectively, in Refs. [40, 41].

For ion-transport simulations ionization-rate coefficients S_{ion} as functions of T_e are necessary; these rates are obtained integrating the $\sigma(E)$ curves over a Maxwell electron-energy

distribution. For an analytical integration, one must use suitable fits to the data. The four-parameter formula proposed by Younger [42] for direct ionisation (DI) appeared to us to be the more suitable for smoothing the experimental curves,

$$\sigma(\mathbf{E}) = \frac{\mathbf{1}}{\mathbf{uI}} \left[\mathbf{A(1\text{-}1/\ u) + B(1\text{-}1/\ u)^2 + CLn(u) + DLn(u)/u}\right] \quad (1)$$

where u=E/I is the ratio between E and the ionisation potential I.

Fits with formula (1) can be used for the experimental ionisation cross sections when both direct and indirect (e.g., inner-shell excitation followed by autoionisation, ISEA) processes are superposed, but ISEA edges are missing. The theoretical Younger's formula requires A and C to be positive and B and D negative. However, this constraint does not apply in our case, when formula (1) is just for fitting data. When ISEA edges occur the experimental curve is extrapolated above the edge in some way homothetically with theoretical DI curves and fitted with formula (1). The remaining part of the $\sigma(E)$ curve (the ISEA σ_{EA} curve) is fitted with the formula proposed for ISEA in Ref. [43]. However, since for several ions the E range of the ISEA curve is not very extended, it appeared necessary to add a sixth term with a $(1\text{-}1/u^4)$ dependence. Consequently the fitting formula becomes

$$\sigma_{\mathbf{EA}}(\mathbf{u}) = \frac{\mathbf{1}}{\mathbf{uI_{EA}}}\left[\mathbf{A + B(1-1/u) + C(1-1/u^2) + D(1-1/u^3) + E(1-1/u^4) + FLn(u)}\right] \quad (2)$$

where now $u=E/I_{EA}$ is the ratio between E and the ISEA ionisation threshold I_{EA} taken at the 'bump' edge. The procedure followed is shown in figure 1, where, for Kr XVI – XIX (Sc-like to Ar-like ions) from Ref. [38], the blue stars show the experimental cross sections, the red broken curve the extrapolated 'DI' cross sections, the magenta stars the expanded 'ISEA' cross sections fitted by the magenta, full curves. The ISEA 'bumps' (caused by inner-shell excitation of 2s and 2p levels), are real, since they are well above the range of the quoted uncertainties on $\sigma(E)$, typically $2\text{-}3\times10^{-20}$ cm^2. For the other, less-ionised ions considered in Ref. [38] possible ISEA 'bumps' are below the reported uncertainties and are consequently neglected.

In figures 2 to 4 the black full curves show the chosen fits of the available experimental data for $\sigma(E)$ ($\sigma(E) + \sigma_{EA}(E)$ for Kr XVI - XIX). The colour curves show the various data available that were used for the fits, the references from which they were taken are given in the captions. When there are differences between the data (e. g., Kr II – V), lacking any preference criterion, the black curves represent the average of the individual fits. We must remark that the differences between the various curves for the same ion can be outside the error bars of the individual measurements. For Kr I (Fig. 2) the theoretical blue chain curve [41], with a larger maximum value, has not been considered, whereas the experimental data from Ref. [28] are not plotted being almost superposed to the black curve. Moreover, it must be observed that, with the single exception of neutral Kr, the complete ionisation calculations reported in Ref. [21] can be considered always in good or fair agreement with either the experimental data or with other theoretical calculations (e.g., Refs. [44, 45]).

The four fit parameters for DI (in units 10^{-14} cm^2 eV^2) are given in table I, along with the ionisation potentials I (in eV). Their values are chosen empirically before the fits and are determined for each ion in such a way that the fitted curve, starting at u=1, follows well the increase of the experimental data. The given I values can be smaller than the ground state ionisation potentials I_g found in the literature, due to the presence in the ion source of populated metastable levels with lower ionisation potentials. As a consequence of the choice of I, the small features caused by metastables in the threshold region are excluded from the fits (the clearest example being Kr IX in figure 3). When $I<I_g$ it is not possible to give a general assessment that quantifies how much contribution to the total measured cross section comes from levels other than the ground level. Each ion constitutes a particular case and is treated in the original references when discussing the experimental data.

The six fit parameters for ISEA (in units 10^{-16} cm^2 eV) are given in table II, along with the ISEA ionisation potentials I_{EA} (in eV) taken at the edge, or rather, at the discontinuity of $\sigma(E)$.

The metastable-level population is related to the electron density n_e in the ion source; levels above the ground state are populated (and de-populated) through electron collisions. Unfortunately, the electron density in these sources is highly uncertain and device dependent; it is guessed to be in the 10^{11} - 10^{12} cm^{-3} range rather than directly measured. In MCF devices typical n_e values are roughly two orders of magnitude higher, and metastable levels are populated. On the other hand, for astrophysicists the contributions of metastable levels to the experimental data are a serious problem since, generally, the n_e values with which they are involved are much lower than those in the ion sources. If the metastable contribution cannot be subtracted, astrophysical modellers tend to prefer theoretical data. Since our calculations are planned for impurity simulations in MCF devices, we propose to use always the experimental data when available. Our decision is supported by the fact that Pindzola et al. [46, 47], in their corresponding reviews of Fe and Ni ionisation data, recommend also the experimental data, even if a clear contribution of metastables is present.

2.2 Molybdenum ions

For molybdenum, experimental $\sigma(E)$ are available for Mo II – IX [48-50], whereas for neutral Mo two theoretical calculations have been found in Refs. [40, 41]. Data for these nine ions have been fit according to formula (1). We must underline that for simplicity we have considered implicitly in the text neutral Mo as having experimental data. In figure 5 the black full curves show the chosen fits for $\sigma(E)$. As with Kr, the colour curves show the various data available used for the fits, the references from which they were taken are given in the captions. No ISEA `bump' is evident for these ions, in spite of the fact that both direct and indirect processes can contribute to their $\sigma(E)$. The four fit parameters for DI are given in table III, along with the ionisation potentials I, obtained as previously explained for Kr.

3. Ionisation rate coefficients

3.1 Krypton ions

For all the ionisation cross sections fitted above, the direct ionisation rate coefficients $S_{ion}(T_e)$ (in units of cm^3/s) are obtained as function of T_e according to the following formula:

$$\mathbf{S_{ion} = 6.69\ 10^{7}\ \frac{\exp(-x)}{T_e^{3/2}}\ F(x)} \qquad (3)$$

where $x = I / T_e$ (both in eV) and

$$\mathbf{F(x) = A\left[1 - x\, f_1(x)\right] + B\left[1 + x - x(2 + x)\, f_1(x)\right] + C f_1(x) + D\, x f_2(x)} \qquad (4)$$

with the four fitting parameters in units 10^{-14} cm^2 eV^2 and the functions $f_1(x)$ and $f_2(x)$ given by

$$\mathbf{f_1(x) = e^x \int_1^\infty \frac{dt}{t} e^{-tx} \qquad f_2(x) = e^x \int_1^\infty \frac{dt}{t} e^{-tx}\, Ln(t)} \qquad (5)$$

For ISEA the ionisation rate (in units of cm^3/s) is

$$\mathbf{S_{ISEA} = 6.69\ 10^{7}\ \frac{\exp(-x)}{T_e^{1/2}}\ F_2(x)} \qquad (6)$$

where now $x = I_{EA} / T_e$ (both in eV) and $F_2(x)$ is given by

$$\mathbf{F_2(x) = A + B[1 - x f_1(x)] + C[1 - x(1 - x f_1(x))] + D\left[1 - 0.5(x - x^2 + x^3 f_1(x))\right]} \\ \mathbf{+ E\left[1 - (x - x^2/2 + x^3/2)/3 + x^4 f_1(x)/6\right] + F\, f_1(x)} \qquad (7)$$

with the six fitting parameters in units of 10^{-16} cm^2 eV.

Since Loch et al. [21] presented tables of S_{ion} for all 36 Kr ions, interpolated values from that work have been taken as reference for comparison with rate coefficients obtained from integrating the experimental cross section data over a Maxwell electron-energy distribution. For several ions up to Ar-like Kr XIX in figures 6 and 7 the black full curves are obtained using formula (3), whereas the blue broken ones are the interpolated total-ionisation

rates from Ref. [21] (the crosses and the stars showing, respectively, the DI and ISEA contributions in the tabulated data). Four ions (Kr II – IV and Kr VI) with practically superposed full and broken curves are not shown, whereas for neutral Kr, as already mentioned when discussing the ionisation the cross sections, the theoretical rate coefficients are two times larger than the experimental ones. In figure 6, for comparison, are also plotted (magenta squares) the S_{ion} values from Mandelbaum et al. for Ge-like Kr V [51] and (magenta circles) the S_{ISEA} values from Mitnik at al. [52, 53] for Zn-like Kr VII and Cu-like Kr VIII.

In Ref. [5] DI ionisation rates coefficients for Kr XXIV – XXXVI (Al-like to H-like ions) and ISEA rate coefficients for Kr XXI - XXVI (S-like to Na-like ions) can be found . For ISEA of Kr XXI – XXIII there is good agreement with Ref. [21] for Kr XXI - XXIII. In figure 8 the various rate coefficients are compared for Kr XXIV – XXVI (blue curves from Ref. [21] and red curves from Ref. [5], with more details in the captions) Differences (increasing in the keV range) are evident for Mg-like and Na-like, particularly for ISEA.

For Kr XXVII-XXXVI (Ne-like to H-like ions) a third calculation is considered with S_{ionL} (in units of cm^3/s) from the well-known Lotz's reference formula [54]

$$\mathbf{S_{ionL} = 6.69 \times 10^{7}\ (aq / T_e^{3/2})\ (expint(x) / x)} \qquad (8)$$

where $a=4.5\ 10^{-14}\ cm^2\ eV^2$, q is the number of equivalent, peripheral electrons with ionisation potential I (given in table IV, taken from Kelly's compendium [55]), $x= I / T_e$ (both in eV) and a second term added to include the ionisation of the two, inner 2s electrons for Ne-like to B-like ions. However, lacking the corresponding inner-shell ionisation potentials, they are taken as approximately equal to the peripheral I-value for Be-like ions (i.e., when the inner electron becomes peripheral). It is a known overestimate, decreasing with decreasing number of peripheral electrons, when the relative inner-electron contribution is increasing. The rates evaluated following formula (8) agree well with the rates from both Ref. [21] and from Ref. [5]. This is shown in figure 8 where the rates of three highly ionised Kr ions are compared with blue full, red broken and black chain curves, respectively, from Refs [21, 5] and according to formula (8). The last comparisons of figure 9 show that Lotz's formula could be used for the same sequences of Mo ions.

When experimental data are available (i.e., from Kr I up to Kr XIX with the exception of Zn-like Kr VII) formula (3) is used with fit parameters from table I, along with formula (6) with fit parameters from table II for the ISEA contribution. For the remaining ions we suggest using S_{ion} rates from Ref. [21] fitted (in units of cm^3/s) with the following formula

$$\mathbf{S_{ionf} = (10^{-11} / T_e^{1/2}) \sum_i C_i\ exp(-E_i / T_e)} \qquad (9)$$

where the fit parameters are given in table V and T_e is in eV. The sum is over terms of the kind used previously to Lotz's formula (see, e. g., Ref. [56]). The number of parameters C_i and E_i

needed for a good fit depends on the T_e range of interest; we consider the range where the fractional abundances $f_Z(T_e)$ at ionisation equilibrium are larger than $10^{-4} - 10^{-3}$.

3.2 Molybdenum ions

Mo ions are treated in the same way as explained previously for the Kr ions. For Mo I-IX, the rate coefficients S_{ion} are evaluated following formula (3) with the fit parameters in table III and three of them (Mo VII-IX) are shown in figure 9 (black full curves). Ionisation rate coefficients for Mo VII-XIV (Kr-like to Cu-like) have been calculated by Mitnik et al [52, 53, 57, 58] and fitted with formula (9) with fit coefficients given in table VI. A few of these coefficients are shown in figure 9 (red, broken and chain curves, respectively, for total and ISEA rates). It appears clearly that for these ions the ratio DI/ISEA increases with the number of peripheral n=4 electrons. Supplementary calculations for Mo XI-XII [51, 59] are also included in figure 9 (blue, stars and circles, respectively, for total and ISEA rates). The black curves from experiments, particularly for Mo VII, are above the theoretical red ones. It is not possible, at the present, to say if the discrepancy is due to the presence of populated metastable levels in the ion sources or to inadequacy of the theory

DI data are available from Ref. [6] according to formula (9) for Mo XV - XXXIII (Ni-like to Ne-like), but ISEA is available only for Mo XXIV-XXXII (K-like to Na-like ions) [60]. Table VII lists the coefficients, where the first pair of numbers is for DI and the second for ISEA. When ISEA is missing, the comparison between DI and ISEA contributions for the Kr ions of the same iso-sequences, i.e. Kr IX – XVII, (see figures 6 and 7) indicates that DI is always the dominating process. Consequently, while waiting for future calculations, we think that we are justified for Mo transport simulation to neglect ISEA for Mo XV-XXIII (Ni-like to Ca-like). As mentioned previously, when discussing the rates of highly ionised Kr ions, for Mo XXXIV-XLI Lotz's formula can be used, with the same general parameter $a=4.5\ 10^{-14}$ $cm^2\ eV^2$ and with I-values from Ref. [61], which are also given in table IV. For H-like Mo XLII experimental cross sections are reported in Refs. [62, 63] in the 30-100 keV range. In this range they are larger than predicted by the Lotz's formula, but they agree with the cross section evaluated by Shi et al. [64], which studied ionisation of the H-like sequence up to Mo. Their cross sections have been fitted with formula (1) (the parameters are also given in table III). It is observed that the two cross sections agree below 40 keV. Since in the hottest MCF devices at present the central electron temperature is, at maximum, around 10 keV, both formulae give similar values for S_{ion} in the T_e range of interest.

4. Recombination rate coefficients

4.1 Radiative recombination

As already discussed in the introduction for recombining Na-like to fully stripped Kr and Mo ions fitting parameters (A, b, T_0 and T_1) of the Verner-Ferland's formula [65], are available

on the University of Strathclyde web site [23]. The recombination rate coefficient α_r (in units of cm^3/s), with T_e in eV, is given by

$$\alpha_r = A \left[\sqrt{\frac{T_e}{T_0}} \left(1+\sqrt{\frac{T_e}{T_0}}\right)^{1-b} \left(1+\sqrt{\frac{T_e}{T_1}}\right)^{1+b} \right]^{-1} \qquad (10)$$

The four parameters required for equation 10, as found on the University of Strathclyde web site (up-dated fits C-20051227), for Kr and Mo are given in table VIII. Tabulated coefficients for the ground states are given [24]. In figure 10, these rates are plotted (blue full curves) for six recombining Kr ions and compared with the approximated rates (red broken curves). For the other six recombining Kr ions and for the corresponding Mo ions the discrepancies are similar, the maximum differences being for the recombining Na-like and Ne-like ions.

For less ionised ions, lacking specific calculations, only a crude approximation is available: recombination processes have been treated separately for recombination into the non-hydrogenic partially filled valence shell and recombination into excited H-like shells (see e.g., the review article by De Michelis & Mattioli [27]). We feel justified to use for the other, less-ionised ions the approximate calculations, all fitted following formula (10), with fitting parameters given in table VIII.

4.2 Dielectronic recombination

As already discussed in the introduction, for recombining Na-like to H-like Kr and Mo ions, fitting parameters are available in the University of Strathclyde web site [23]. The recombination rate coefficient α_d (in units of cm^3/s), with T_e in eV, is given by

$$\alpha_d = \frac{1}{T_e^{3/2}} \sum_i C_i \exp\left(-\frac{E_i}{T_e}\right) \qquad (11)$$

the C and E parameters are listed in table IX for Kr and Mo, with enough of each coefficient to use the formula down to the low-temperature regime of photoionised plasmas. The given parameters (up-dated fits C-20060311) refer to the DR totals of the ground level. In this last web file N. Badnell included fit coefficients for DR totals from the lowest excited levels. At photoionised plasma temperatures, these can be quite different from the ground level results. On the other hand, for electron temperatures typical of electron-collision-dominated plasmas the differences between ground and excited level (within the ground term) are generally not greater than 10-20%.

The rate coefficients using the C and E parameters in table IX (blue full curves) are compared with revised data from Refs [5, 6] (red broken curves for recombining Kr

and Mo ions from Na-like to H-like. In figures 11 and 12 rates six of these recombining ions are presented, respectively for Kr and Mo. Comparison with other available calculations [66-78] are included and detailed in the captions. In Ref. [60] coefficients C and E are also given for recombining Mo ions down to Ar-like. For other, less-ionised ions we found specific calculations in the literature for recombining Na-like and Mg-like [78], and for recombining Ni-like ions [79, 80]. For all the other ions, only the BM formula, summed over two resonance transitions (a $\Delta n=0$ and a $\Delta n=1$) of the recombining ion, is available. It is known that this formula underestimates the DR rates at low T_e; it neglects low lying autoionising states since the mean thermal energy of the free electrons is assumed to be at least comparable to the excitation energy of the first resonance transitions of the recombining ion. This has been discussed in detail by Savin et al. [81, 82] and the reader should refer to their papers. At the present, the BM formula is found to be marginally satisfactory for electron-collision-ionised plasmas (i.e., for MCF devices), but not for the low temperature astrophysical photoionised plasmas.

For recombining Al-like to Ar-like Kr ions we have used the BM formula oscillator strengths f and excitation energies E_{ex} of the resonance transitions (required for the BM formula), which are obtained by extrapolation of the corresponding values used for ions of elements up to Ge in Ref [2]. On the other hand, for Mo in Ref. [60] fit parameters are given down to recombining Ar-like ions. For ions less charged than the Ar-like charge state of both elements, f and E_{ex} values were found in the Appendix of Post et al. [3]. Since the average-ion-model energies given by the their code (Adpak) were not available to us, the excitation energies have been taken to be H-like in the oscillator strength $f_{n,n+1}$ formula (see page 436 of [3]). Moreover, for Mo, Mitnik [57] evaluated f and E_{ex} for recombining Mo V to Mo XIX (Sr-like to Cr-like) and these values are preferred to the ones from Adpak. Comparisons of DR rate coefficients for a few Mo ions are shown in figure 13. For Mo XXXI (Mg-like) $\alpha_d(T_e)$ curves from Refs. [60, 78] are compared (red full curve and green broken curve respectively). For the other ions the adopted $\alpha_d(T_e)$ blue curves (full curves, circles and crosses, respectively, for total, $\Delta n=1$ and $\Delta n=0$ rates) are compared with the corresponding red curves from Adpak (broken curves, squares and stars, respectively, for total, $\Delta n=1$ and $\Delta n=0$ rates). Considering all the ions treated by Mitnik [57], it appears that Adpak is satisfactory for recombining Co-like to Cr-like ions. On the other hand, for recombining Sr-like to Cu-like ions the f and E_{ex} values proposed by Mitnik predict a larger 'T_e threshold'. As already said, Mitnik's calculations are preferred to the general ones from Adpak. For recombining Ni-like ions (with only $\Delta n=1$ transitions) Behar's data (green chain curve) [78,79] are preferred. For all the lowly ionised isosequences of both Kr and Mo, the C and E coefficients obtained from fits to formula (9) are given in table IX, they have been obtained by limiting the minimum temperature in such a way that the fractional abundances of the considered ion was in the range 10^{-4} - 10^{-3}.

5. Ionisation balance and conclusion

In the previous sections we have presented the data on recombination and ionisation of Kr and Mo ions and the proposed fit coefficients (tables I – IX). When experimental ionisation cross sections were available (Kr I - VI, Kr VIII – XIX and Mo I-IX) the ionisation rate coefficients have been obtained by integration over a Maxwellian electron distribution (tables I - III). For the remaining Kr ions the fitted rate coefficients are tabulated in Ref. [21] for all the 36 ions should be used (table V). For Mo the corresponding rate coefficients for the 42 Mo ions are not available at the moment. The proposed data are from Mitnik et al. [52, 53, 57, 58] for Mo X – XIV (As-like to Cu-like ions in table VI) and from LLNL computations [6, 60] for Mo XV - XXXIII (Ni-like to Ne-like ions in table VII). The contribution of ISEA is missing for Mo XV – XXIII (Ni-like to Ca-like), but it can be neglected for these sequences by comparison with the calculations for the corresponding Kr IX – XVII. For Mo XXXIV – XLII (F-like to H-like) Lotz's formula (8) can be used.

For RR and DR the recommended data are given, respectively, in tables VIII and IX. For highly ionised recombining ions from bare or H-like down to the Na-like sequence the data available on the University of Strathclyde web site [23] from the coordinated programme are given. For RR of the lowly ionised ions the simple, coarse approximation of recombination into a partially filled valence band and into H-like excited levels is considered [27]. For DR of the lowly ionised ions the general BM formula is used [25, 26] except in cases where a few, detailed calculations exist.

The proposed data allow straight-forward determination of the CSD at ionisation equilibrium, i.e., the ionic fractions or fractional abundances f_Z as function of T_e. Tables of f_Z (Te) are given (X and XI), respectively for Kr and Mo.

Only ionising electron collisions and radiative and dielectronic processes have been considered. The neglected processes are photoionisation, photoabsorption, electron-impact multiple ionisation, three-body recombination, electron-density effects both in ionisation and in dielectronic recombination and, finally charge-exchange (CX) reactions of the plasma ions with neutral-hydrogen isotopes. Except for the last two, these processes can be neglected in MCF devices. CX reactions reduce the ionisation degree and represent a supplementary recombination process included, if necessary, in the simulation codes. For the two elements considered in this paper only scaled cross sections versus scaled energies are available (see, e.g., the references quoted in the last section of Ref. [2]). Multiple ionisations, for which experimental data exist for a few lowly ionised Kr and Mo ions, can be neglected in MCF devices. This has been shown in the simulations of Ref. [83] to be due to the fact that, at the edge, the ions are located in layers with T_e values near the single-ionisation potentials and multiple ionisation has a larger threshold. On the other hand, if neutrals or lowly ionised ions are suddenly exposed to high T_e values, multiple ionisations could influence the charge-state evolution. This is possible in MCF devices with laser blow-off or pellet impurity

injections, but no reliable spectroscopic measurements on the localised interaction region are available.

The necessity of corrections to the proposed DR rates is in some way an open question. The rates are first decreased by ionisation of the singly excited states, i.e. the non-autoionising states following stabilisation; they are then decreased with increasing n_e. Moreover, as shown in Ref. [84], there is some enhancement due to l-mixing of autoionising states by electric field (Stark effect) and/or by collisional redistribution of population, but probably not enough enhancement to bring it back to the zero-density value. The influence of the electric field has been clearly observed in several DR experiments, but the plasma microfields or turbulent fields are hardly known. The picture is further complicated by the discovery that magnetic fields, crossed with electric fields, reduce, in most cases. the electric-field enhancement [22]. A correction formula for the n_e influence had been proposed a long time ago in Ref. [3], but, as far as we know, at the present, the DR rates included in simulation codes do not consider any influence of the electron density or that of the electric fields. The corresponding effect on the ionisation rates, which are increased through ionisation of the excited states, is considered marginal at the densities of MCF devices.

To conclude, we believe that the data collected here represent the state of the art for ionisation and recombination data of Kr and Mo ions. Sets of rates are proposed that should be used in simulation codes to evaluate the ionisation balances of Kr and Mo in MCF devices and to compare them with experimental results.

Acknowledgements

One of the authors (MM) wishes to thank Prof. Nigel Badnell for many useful interactions through e-mails and for placing him on the mailing list for announcing new releases on the University of Strathclyde web site. This work was performed under the auspices of the U.S. Department of Energy by University of California, Lawrence Liver -more National Laboratory under Contract No. W-7405-ENG-48.

References

[1] Mazzotta P, Mazzitelli G et al 1998 Astron. & Astrophys. Suppl. **133** 403
[2] Mazzitelli G and Mattioli M 2002 At. Data Nucl. Data Tables **82** 313
[3] Post D, Jensen R et al 1977 At. Data Nucl. Data Tables **20** 397
[4] Post D, Abdallah J. et al 1995 At..Phys. Plasmas **2** 2328
[5] Fournier K, May M et al 2000 Nucl. Fusion **40** 847
[6] Fournier K, Pacella D et al 1997 Nucl. Fusion **37** 825 (Erratum 1998 **38** 639)
[7] Ongena J, Messiaen A et al 1999 Plasma Phys. Control. Fusion **41** A379
[8] Maddison G, Brix M et al 2003 Nucl. Fusion **43** 49
[9] Jackson G, Murakami M et al 2002 Plasma Phys. Control. Fusion **44** 1893
[10] Rapp J, Tokar M et al 1997 Plasma Phys. Control. Fusion **39** 1615

[11] May M, Fournier K et al 2000 Phys. Rev. E **61** 3042
[12] May M, Fournier K et al 1999 Plasma Phys. Control. Fusion **41** 45
[13] Philipps V, Tanabe T. et al 1994 Nucl. Fusion **34** 1417
[14] Rice J, Terry J et al 1996 J. Phys B. At. Mol. Opt. Phys. **29** 2191
[15] May M, Finkenthal M et al 1997 Nucl. Fusion **37** 881
[16] Carraro L, Gabellieri L et al 2004 Plasma Phys. Control. Fusion **46** 389
[17] Pacella D, Fournier K et al 2000 Phys. Rev. E **61** 5701
[18] Mattioli M, Carraro L et al 2004 31st EPS Conf. on Plasma Phys., London, ECA **28G** P-1.150
[19] Dux R, Peeters A et al 1999 Nucl. Fusion **39** 1509
[20] Dux R, Giroud C et al 2004 Nucl. Fusion **44** 260
[21] Loch S, Pindzola M et al 2002 Phys. Rev. A **66** 02708
[22] Badnell N, O'Mullane M et al 2003 Astron.& Astrophys. **406** 1151
[23] http://amdpp.phys.strath.ac.uk/tamoc/DR or /RR
[24] Badnell N submitted to Astrophys. J. Suppl.
[25] Burgess A 1965 Astrophys. J. **141** 1588
[26] Merts A, Cowan R and Magee N 1976 Los Alamos Report LA-6260-MS
[27] De Michelis C and Mattioli M 1981 Nucl. Fusion **21** 677
[28] Krishnakumar E and Srivastava S 1988 J. Phys. B: At. Mol. Opt. Phys. **21** 1055
[29] Wetzel R, Baiocchi F at al 1987 Phys. Rev. A **35** 559
[30] Man K, Smith A and Harrison M 1987 J. Phys. B: At. Mol. Opt. Phys. **20** 5865
[31] Man K, Smith A and Harrison M 1987 J. Phys. B: At. Mol. Opt. Phys. **20** 1365
[32] Tinschert K, Müller A et al 1987 J. Phys. B: At. Mol. Opt. Phys. **20** 1121
[33] Gregory D 1985 Nucl. Instrum. Methods in Phys. Res. B **10/11** 87
[34] Gregory D, Dittner P and Crandall D 1983 Phys. Rev. A **27** 724
[35] Bannister M, Guo X and Kojima T 1994 Phys. Rev. A **49** 4676
[36] Bannister M, Müller D et al 1988 Phys. Rev. A **38** 38
[37] Teng H, Defrance P et al 2000 J. Phys. B: At. Mol. Opt. Phys. **33** 467
[38] Khouilid M, Cherkani-Hassani S et al (2001) J. Phys. B: At. Mol. Opt. Phys. **33** 467
[39] http://www-cfadc.phy.ornl.gov/xbeam/
[40] Higgins M, Lennon M et al 1989 Culham Laboratory Report CLM-R289, data also available on the ORNL site [39]
[41] Bartlett P and Stelbovics A 2004 At. Data Nucl. Data Tables **86** 235
[42] Younger S 1981 J. Quant. Spectrosc. Radiat. Transfer **24** 1272
[43] Arnaud M and Raymond J 1992 Astrophys. J. **398** 394
[44] Chen M and Reed K 1993 Phys. Rev. A **47** 1874
[45] Gorczyca T, Pindzola M et al 1994 Phys. Rev. A **49** 4682
[46] Pindzola M, Griffin D et al. 1987 Nucl. Fusion Suppl. p 21
[47] Pindzola M, Griffin D et al. 1991 Phys. Scripta T37 35
[48] Man K, Smith A and Harrison M 1987 J. Phys. B: At. Mol. Opt. Phys. **20** 1351
[49] Hathiramani D, Aichele K et al. (1996) Phys. Rev. A **54** 587
[50] Bannister M, Meyer F et al 1995 Phys. Rev. A **52** 413
[51] Mandelbaum P, Cohen M et al 2005 Eur. Phys. J. D **33** 213
[52] Mitnik D, Mandelbaum P et al 1996 Phys. Rev. A **53** 3178
[53] Mitnik D, Mandelbaum P et al 1997 Phys. Rev. A **55** 307
[54] Lotz W 1968 Z. Physik **216** 241

[55] Kelly R 1987 J. Phys. Chem. Ref. Data **16** Supplement No.1
[56] Jordan C 1969 Mon. Not. R. astr. Soc. **142** 501
[57] Mitnik D, Mandelbaum P. et al. 1994 Phys. Rev. A 50 4911
[58] Mitnik D. PhD Thesis University of Jerusalem (1996)
[59] Oreg J, Goldstein W et al., 1994 Phys. Rev. A 44 1741
[60] Fournier KB, Cohen M, et al. 1996 Phys. Rev. A **54** 3870.
[61] Carlson T, Nestor C et al 1970 Atomic Data **2** 63
[62] Marr R, Elliot S and Scofield J 1997 Phys. Rev. A 56, 1338
[63] Wanatabe H, Currell F et al 2002 .J. Phys. B: At. Mol. Opt. Phys. 35, 5095
[64] Shi X, Chen C et al 2005 J. Quant. Spectrosc. Radiat. Transfer **91** 161
[65] Verner D and Ferland G. 1996 Astrophys. J. Suppl. **103** 467
[66] Nilsen J, 1986 J. Quant. Spectrosc. Radiat. Transfer **36** 539
[67] Nilsen J, 1986 J. Phys. B: At. Mol. Phys. **19** 2401
[68] Chen M, 1986 Phys. Rev. A **33** 994
[69] Chen M, 1991 Phys. Rev. A. **44** 4215
[70] Roszman L 1987 Phys. Rev. A **35** 2122
[71] Chen M, 1988 Phys. Rev. A **38** 5595
[72] Chen M, 1998 Phys. Rev. . **58** 4539
[73] Dasgupta A and Whitney K 1994 Atom. Data Nucl.Data Tables **58** 77
[74] Roszman L, 1987 Phys. Rev. A **35** 3368
[75] Chen M, 1988 Phys. Rev. A **38** 2332
[76] Roszman L, 1987 Phys Rev. A **35** 2138 (Erratum 1989 **39** 913)
[77] Chen M, 1986,Phys. Rev. A **34** 1073
[78] Hahn Y,1993 J. Quant. Spectrosc. Radiat. Transfer **49** 81 (Erratum 1994 **51** 663)
[79] Behar E, Mandelbaum P and Schwob J L 1996 Phys. Rev. A **54** 3070
[80] Behar E, Doron R et al 1998 Phys. Rev. A **58** 2115 (1998)
[81] Savin D, Kahn S et al 1999 Astrophys. J. Suppl. **123** 687
[82] Savin D, Kahn S et al 2003, Astrophys. J. Suppl. **147** 421
[83] Tendler M, Lackner K and Wunderiich R 1984 Phys. Lett **106A** 420
[84] Badnell N, Pindzola M et al. 1993 Astrophys. J. Suppl. **407** L91

Figure captions

Figure 1 (from left to right and from top to bottom, units 10^{-17} cm^2 and eV)
Blue full curve: experimental ionisation cross sections $\sigma(E)$ for Kr XVI – XIX: red broken curve: DI cross section $\sigma_{DI}(E)$ extrapolated above the ISEA edge; magenta: expanded ISEA cross section $\sigma_{EA}(E)$, stars experimental points and full curves fits according to formula (2) (Kr XVI *10, Kr XVII *4, Kr XVIII - XIX *3).

Figure 2 (from left to right and from top to bottom, units 10^{-17} cm^2 and eV)
experimental ionisation cross sections $\sigma(E)$ for Kr I-VI,
black full curves: selected fits according to formula (1);

Kr I blue circles [29], green broken [40], blue chain (not considered for the fit) [41], Ref. [28] considered for the fit, but not shown, since quite near to the black curve;
Kr II: red crosses [32], green broken [40]=[30]
Kr III: red crosses [32], blue circles [31], magenta stars [33]=[40];
Kr IV: red crosses [32], magenta stars[34];
Kr V: magenta stars [35], blue crosses [39];
Kr VI: magenta circles [35].

Figure 3 (from left to right and from top to bottom, units 10^{-18} cm^2 and eV)
experimental ionisation cross sections $\sigma(E)$ for Kr VIII - XIII,
black: full curves: selected fits according to formula (1);
Kr VIII: red circles [35], magenta stars [39]; Kr IX: red circles [36];
Kr X: magenta stars [39]; Kr XI - XII: blue crosses [37];
Kr XIII: blue crosses [38].

Figure 4 (from left to right and from top to bottom, units 10^{-19} cm^2 and eV)
experimental ionisation cross sections $\sigma(E)$ for Kr XIV-XIX,
black: full curves: selected fits according to formula (1), including contribution of ISEA according to formula (2) for Kr XVI – XIX;
Kr XIV - XIX: blue crosses [38].

Figure 5 (from left to right and from top to bottom, units 10^{-17} cm^2 and eV)
experimental ionization cross sections $\sigma(E)$ for Mo I - IX
black: full curves: selected fits according to formula (1);
Mo I: green broken [40], blue chain [41]; Mo II: blue crosses [48]=[40], magenta stars [49];
Mo III - IV: magenta stars [49]; Mo V - VI: green circles [50], magenta stars [49];
Mo VII - IX: magenta stars [49].

Figure 6 (from left to right and from top to bottom, units cm^3/s and eV)

ionisation rate coefficients $S_{ion}(T_e)$ for Kr V and Kr VII-XI;
black full curves:: selected fits according to formula (3), excepted for Kr VII;
blue: rates from [21] (broken curves interpolated total rates, crosses DI, stars ISEA with unit autoionisation branching ratio);
magenta: squares Kr V total rate [51], circles Kr VII-VIII ISEA rates [52, 53].

Figure 7 (from left to right and from top to bottom, units cm^3/s and eV)

ionisation rate coefficients $S_{ion}(T_e)$ for Kr XII-XIX;
black: selected fits according to formula (3), including contribution of ISEA according to formula (5) for Kr XVI-XIX;
blue: rates from [21] (broken curves interpolated total rates, crosses DI rates, stars ISEA rates with unit autoionisarion branching ratio).

Figure 8 (from left to right and from top to bottom, units cm^3/s and eV)

ionisation rate coefficients $S_{ion}(T_e)$ for Kr XXIV – XXVII, Kr XXXII, Kr XXXVI;
blue; rates from [21] (full curves interpolated total rates, crosses DI rates, circles ISEA rates with autoionisarion branching ratio different from one)
red: rates from [5] (broken total rates, stars DI rates, squares ISEA rates)

black: chain rates from Lotz's formula (8) for the three more ionised ions.

Figure 9 (from left to right and from top to bottom, units cm^3/s and eV)

ionisation rate coefficients $S_{ion}(T_e)$ for Mo VII – IX, XI – XII, XIV;
black full curves: selected fits according to formula (3), for Mo VII-IX;
red: rates following Mitnik et al [52, 53, 57 ,58] (broken total rates, chain ISEA rates);
blue: stars total rates Mo XI [51] and Mo XII [59], circles Mo XII ISEA rates [59].

Figure 10 (from left to right and from top to bottom, units cm^3/s and eV)

radiative recombination rate coefficients $\alpha_r(T_e)$ for recombining
Kr^{25+},Kr^{26+},Kr^{29+},Kr^{32+},Kr^{34+},Kr^{36+}
blue full curves: rates from [23], red broken curves: rates according to the simplified model of recombination into the non-hydrogenic partially filled valence shell and recombination into excited H-like shells, as explained in Ref [27].

Figure 11 (from left to right and from top to bottom, units cm^3/s and eV)

Dielectronic recombination rate coefficients $\alpha_d(T_e)$ for recombining
Kr^{26+},Kr^{27+},Kr^{29+},Kr^{31+},Kr^{33+},Kr^{35+}
Blue full curves: rates from [23], red broken curves: rates from [5]

references for other colours for the indicated recombining sequences:

Ne-like :magenta circles [77]; F-like magenta circles [75], black chain [76];

B-like magenta circles [72], Li-like magenta circles [69], black chain [70];

H-like black stars [66]

Figure 12 (from left to right and from top to bottom, units cm^3/s and eV)

dielectronic recombination rate coefficients $\alpha_d(T_e)$ for recombining
Mo^{31+},Mo^{33+},Mo^{34+},Mo^{36+},Mo^{38+},Mo^{40+}
Blue full curves: rates from [23], red broken curves: rates from [60]

references for other colours for the indicated recombining sequences;

Na-like black chain [78]; F-like black magenta circles [75] black chain [76],

O-like black chain [74], black crosses [73], Be-like magenta circles [71],

He-like magenta circles [68], black stars [67],

Figure 13 (from left to right and from top to bottom, units cm^3/s and eV)

dielectronic recombination rate coefficients $\alpha_d(T_e)$ for recombining
Mo^{4+},Mo^{10+},Mo^{14+},Mo^{18+},Mo^{23+},Mo^{30+},

blue: rates using BM formula with f and E_{ex} as proposed by Mitnik et al. [57] (full curves total rates, circles $\Delta n=0$ transitions, crosses $\Delta n=1$ transitions);

red: rates using BM formula with f and E_{ex} from Adpak [3] (full curves total rates, squares $\Delta n=0$ transitions, stars $\Delta n=1$ transitions)
for Ni-like ions black chain rates from Behar [79, 80],
for Mg-like red broken and black full, respectively, from Refs [60] and [78]

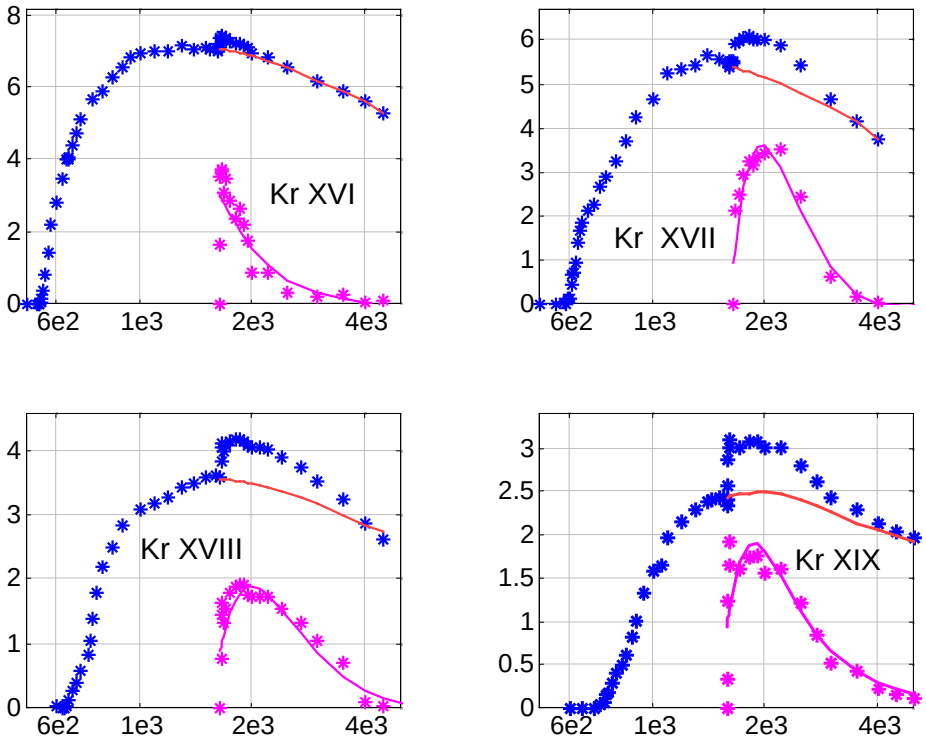

Figure1 **Kr XVI -XIX** σ **(E),** σ_{DI}**(E) extr,** σ_{EA}**(E)** (units 1e-19 cm ^{2}, eV)

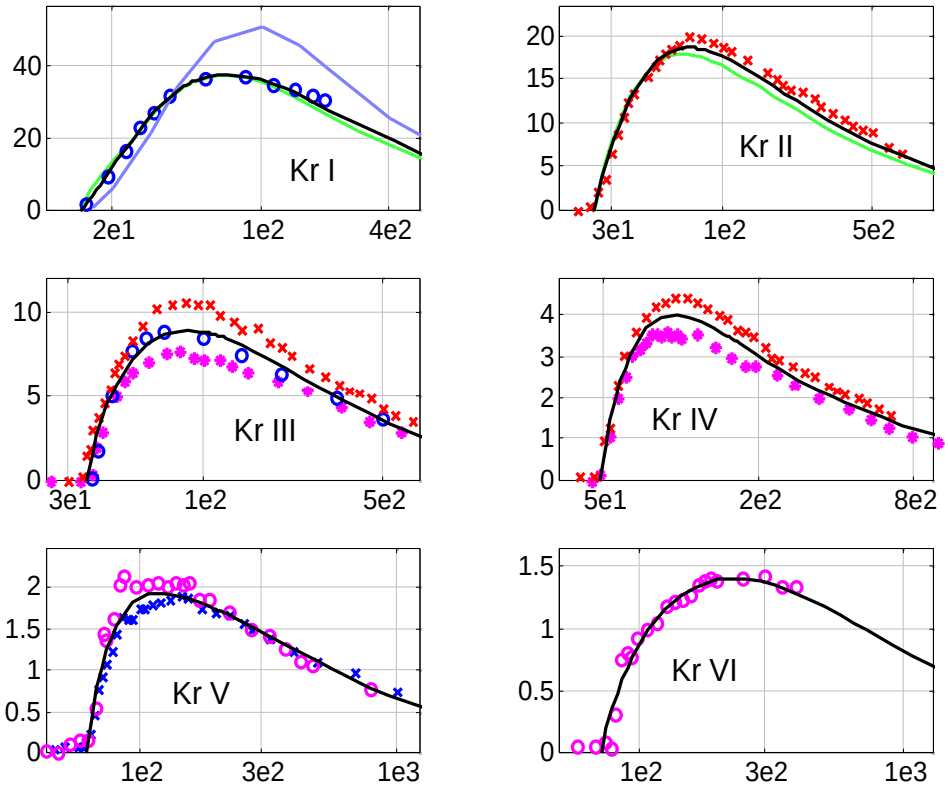

Figure 2 Kr I -VI σ **(E)** (units 1e-17 cm ^{2}, eV)

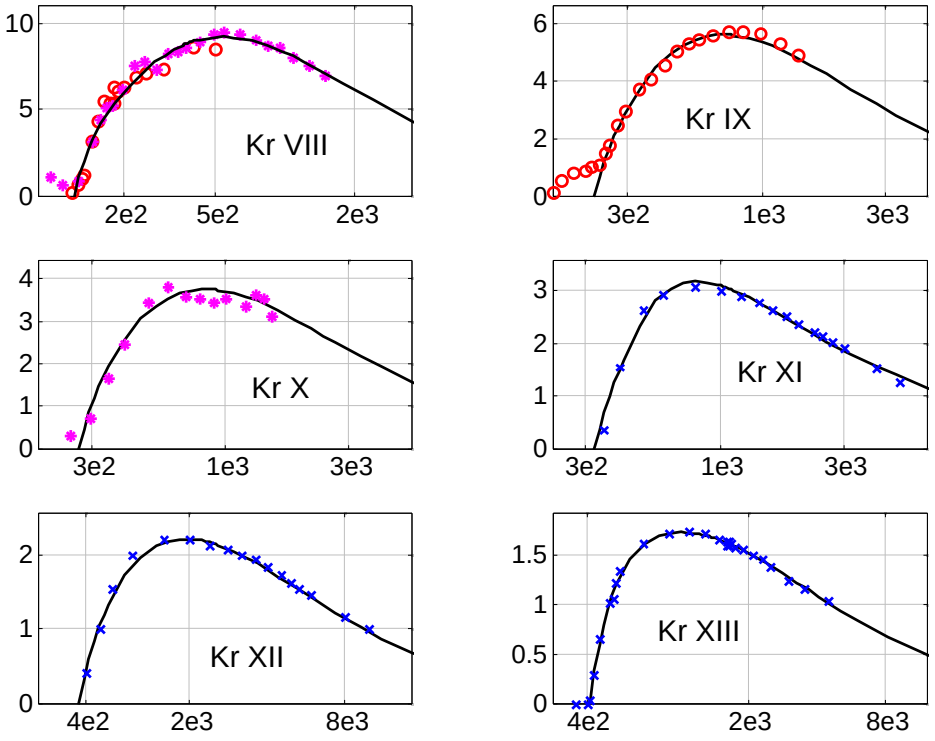

Figure 3 **Kr VIII - XIII** σ **(E)** (units 1e-18 cm ^{2}, eV)

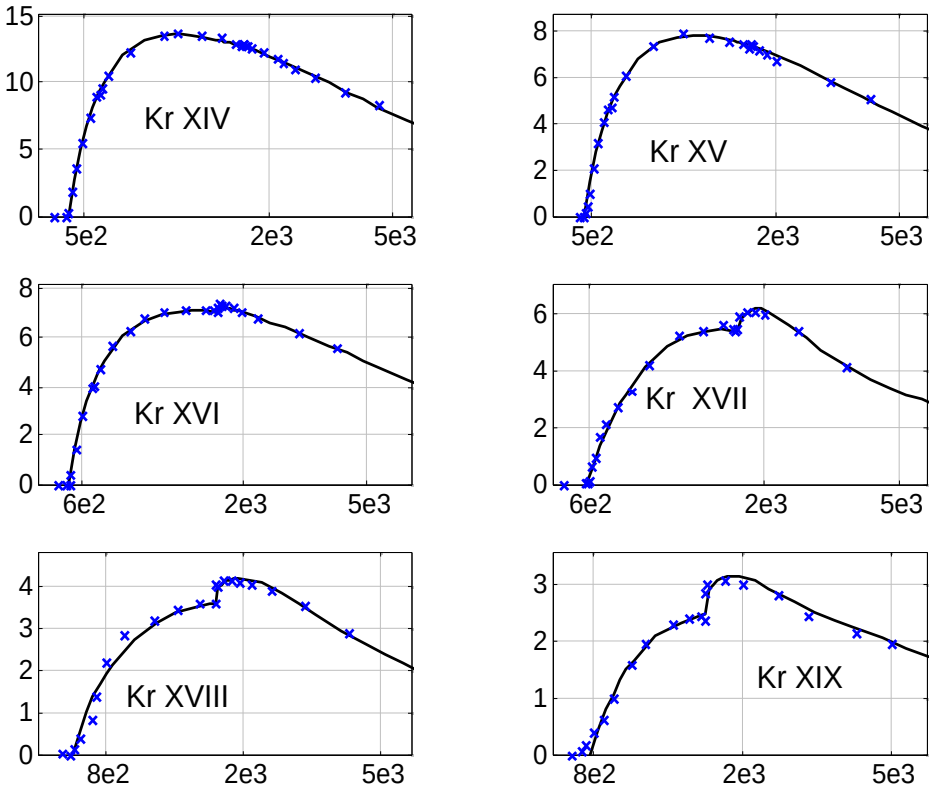

Figure 4 **Kr XIV - XIX** σ **(E)** (units 1e-19 cm ^{2}, eV)

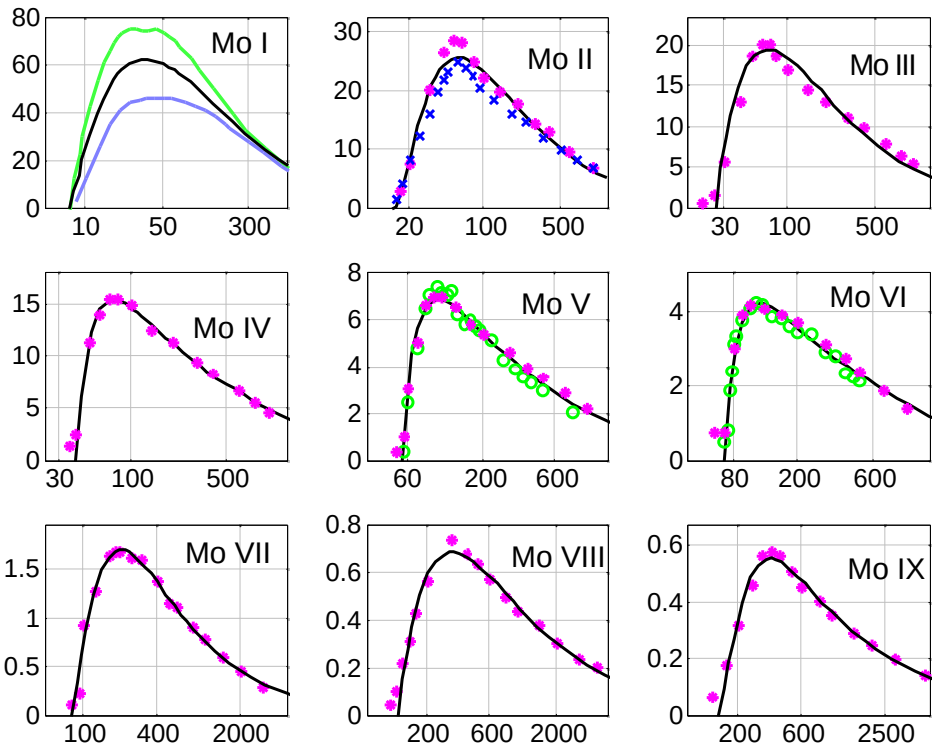

Figure 5 Mo I - IX σ (E) (units 1e-17 cm ^{2}, eV)

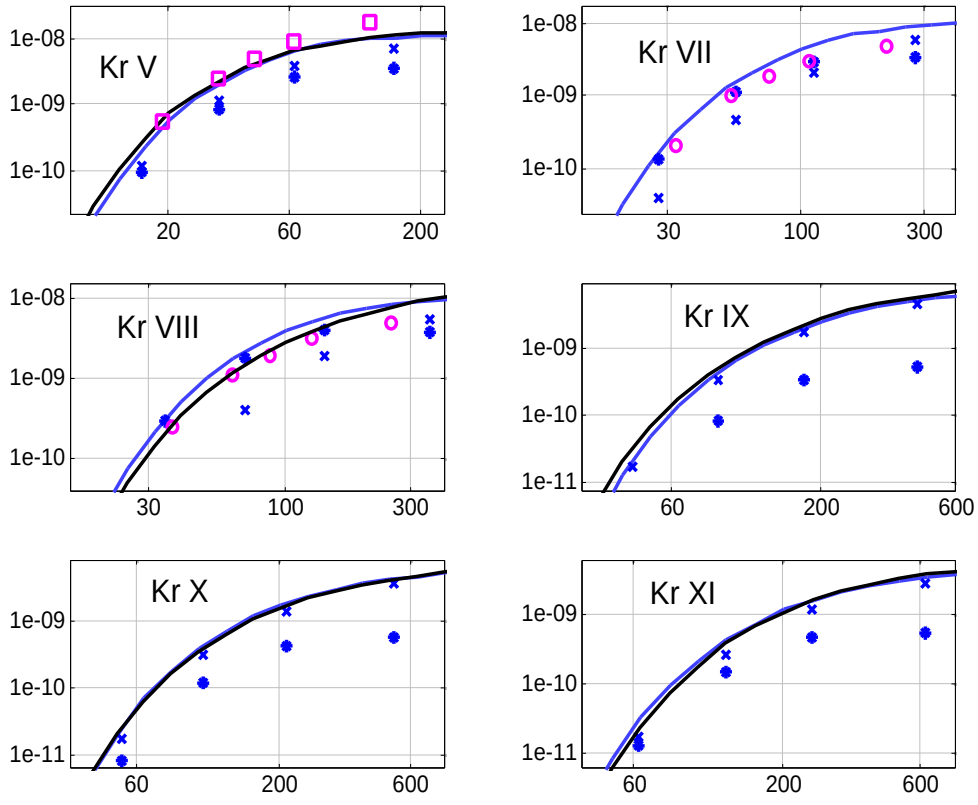

Figure 6 **Kr V + Kr VII - XI** $S_{ion}(T_e)$ (units cm^3/s, eV)

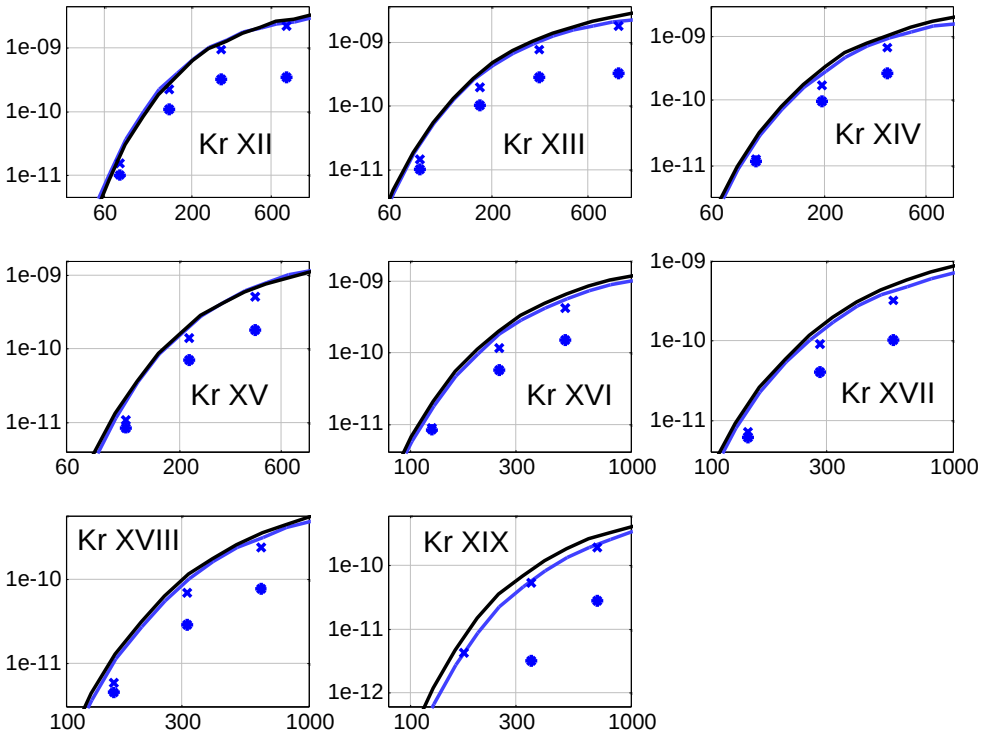

Figure 7 **Kr XII - XIX** $\mathbf{S_{ion}\,(T_e)}$ (units cm^3/s, eV)

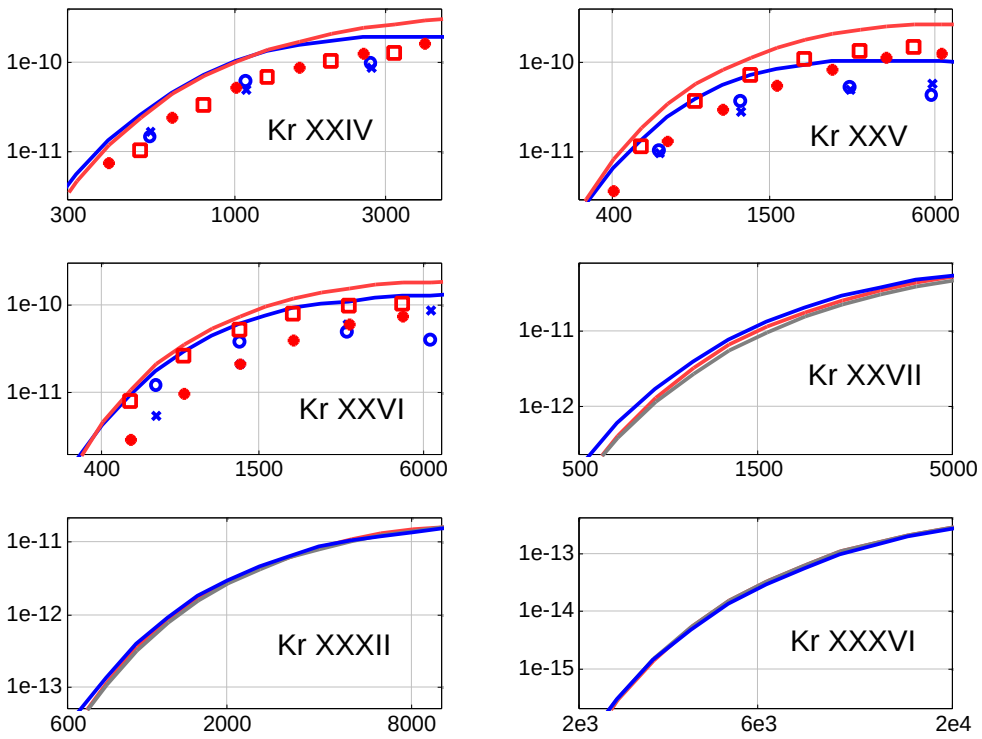

Figure 8 Kr XXIV - XXVII + Kr XXXII + Kr XXXVI $\mathbf{S_{ion}\,(T_e)}$ (units cm^3/s , eV)

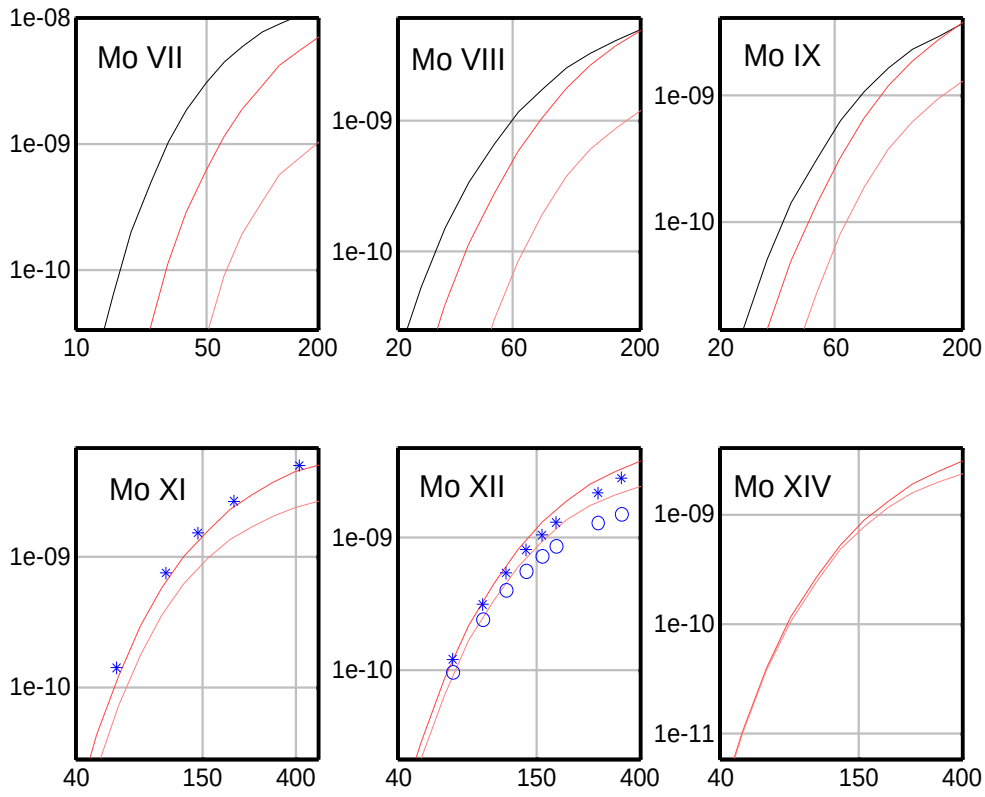

Figure 9 **Mo VII - IX + XI-XII + XIV** $S_{ion}(T_e)$ (units cm^3/s , eV)

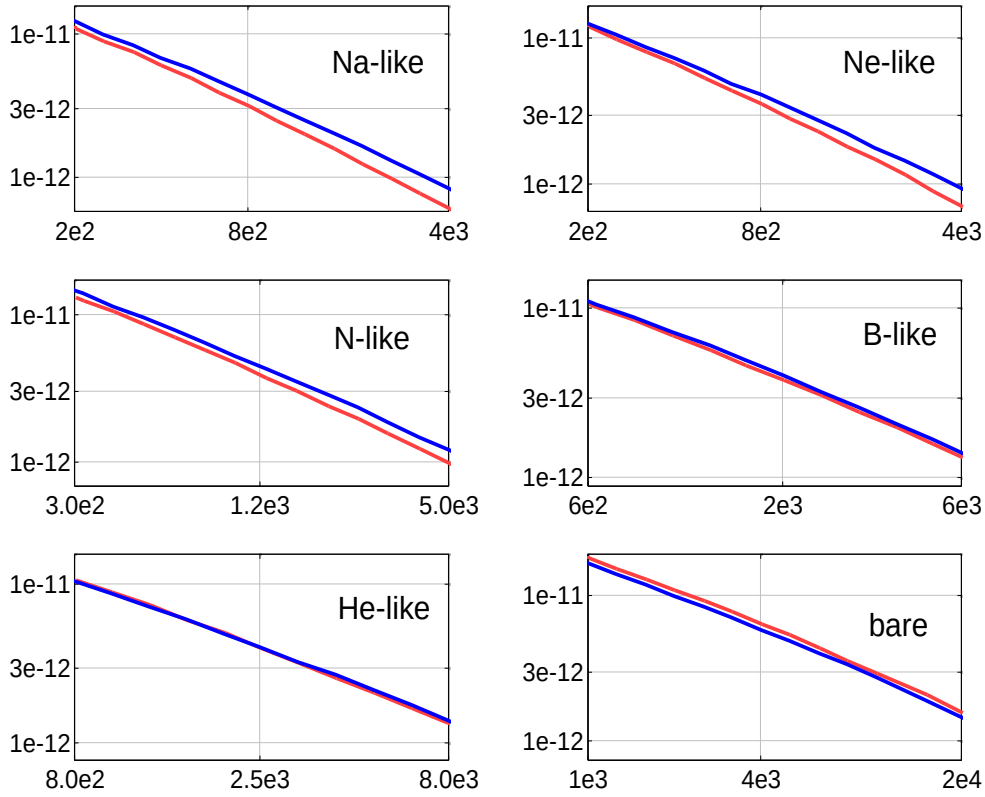

Figure 10 recombining Kr^{25+} - Kr^{26+} - Kr^{29+} - Kr^{32+} - Kr^{34+} - Kr^{36+} $\alpha_r(T_e)$ (units cm^3/s , eV)

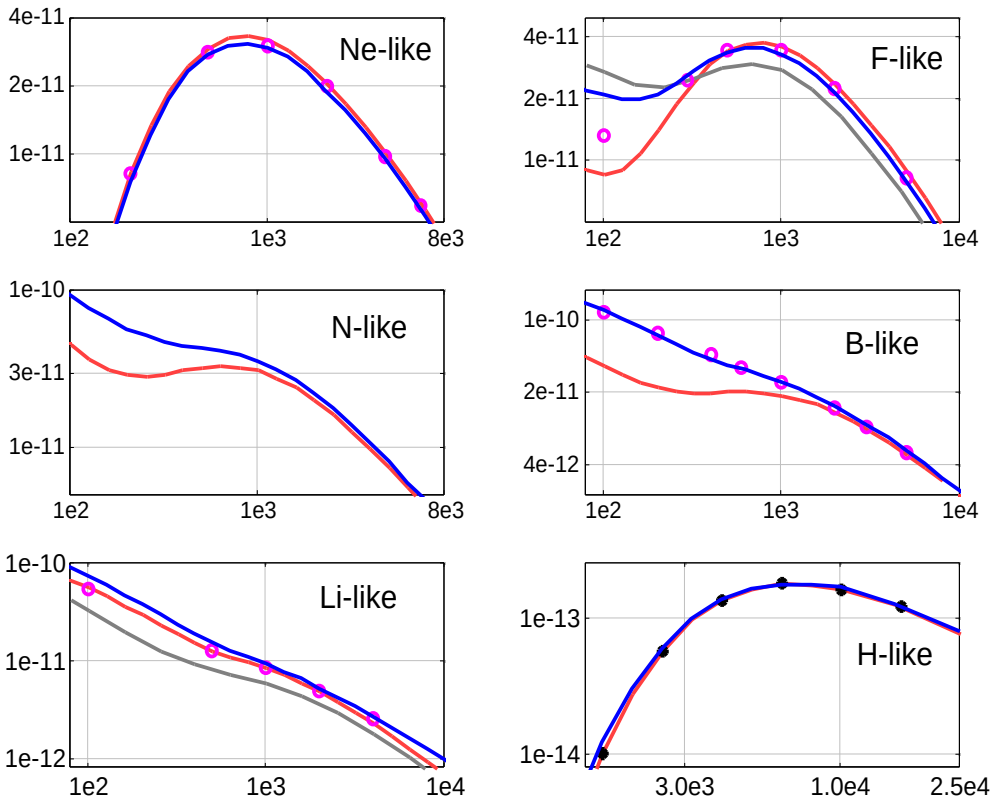

Figure 11 recombining Kr $^{26+}$ - Kr $^{27+}$ - Kr $^{29+}$ - Kr $^{31+}$ - Kr $^{33+}$ - Kr $^{35+}$
$\alpha_d\,(T_e)$ (units cm^3/s, eV)

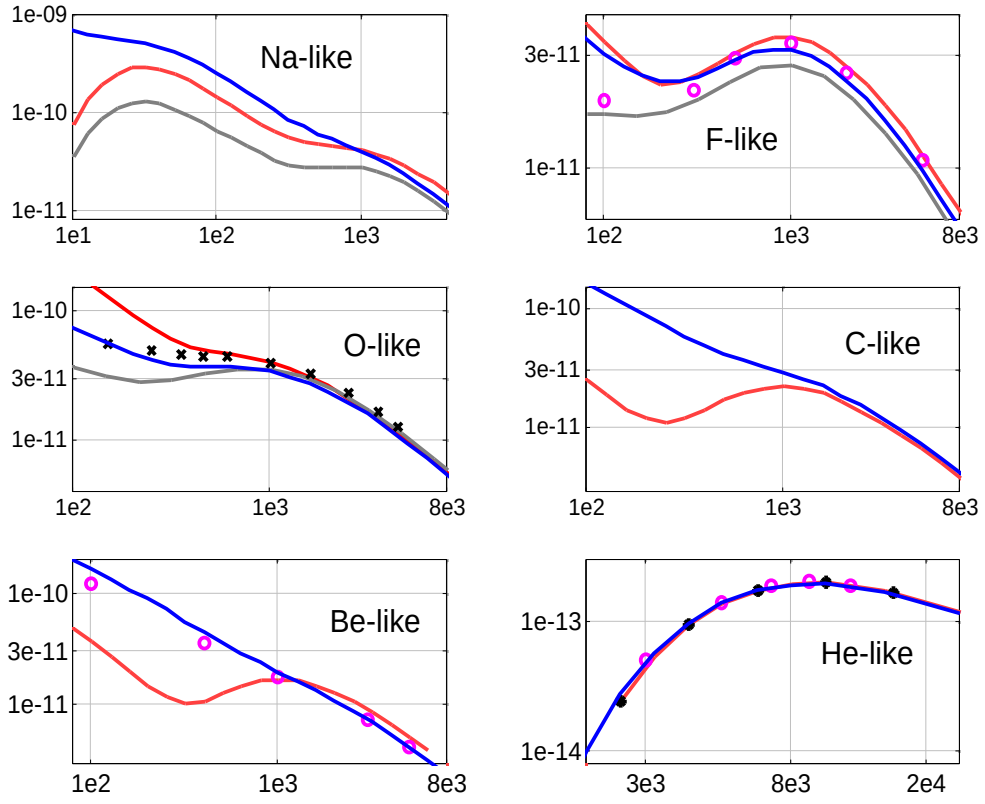

Figure 12 recombining Mo $^{31+}$ - Mo $^{33+}$ - Mo $^{34+}$ - Mo $^{36+}$ - Mo $^{38+}$ - Mo $^{40+}$
α_d **(T$_e$)** (units cm ^{3} /s , eV)

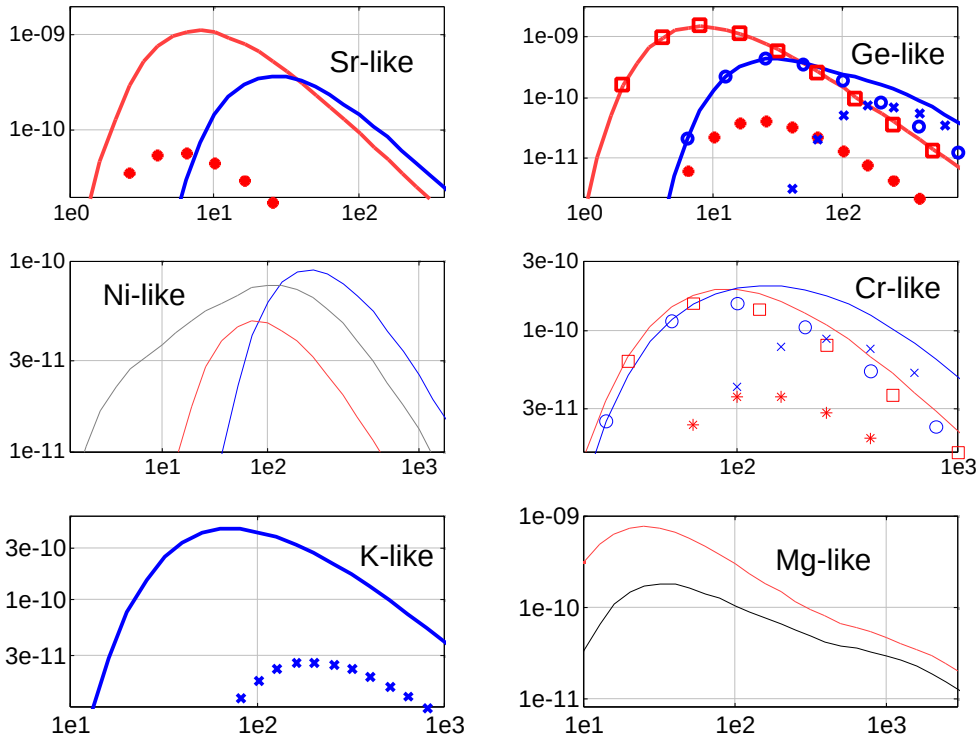

Figure 13 recombining Mo $^{4+,\ 10+,\ 14+,\ 18+,\ 23+,\ 30+}$ $\alpha_d\ (T_e)$ (units cm ^{3} /s , eV)

Table I

Kr ions

fit parameters A, B, C, D (units: 1e-14 cm^2 eV^2)
for evaluating DI ionisation cross sections and rates
according to, respectively, formulae 1 and 3
Z spectroscopic notations and I (eV) ionisation potentials

Z	I	A	B	C	D
1	14.	-35.30	-13.40	47.00	-6.50
2	24.6	-49.50	26.40	37.80	36.90
3	35.	241.20	-96.70	-16.70	-183.50
4	48.	28.90	-23.30	14.80	-1.00
5	62.	163.80	-89.70	-4.70	-119.20
6	72.	96.00	-56.60	13.50	-86.70
8	120.	104.30	-119.00	62.80	-130.40
9	220.	577.40	-253.80	-8.90	-494.60
10	265.	410.60	-191.80	19.20	-356.00
11	320.	-272.20	167.10	103.40	245.60
12	370.	670.60	-263.30	-44.60	-521.70
13	405.	548.80	-309.10	15.70	-439.10
14	445.	472.80	-291.00	25.40	-368.30
15	475.	313.20	-174.80	7.80	-239.90
16	540.	260.20	-203.70	53.20	-217.60
17	585.	226.90	-69.76	-3.80	-166.40
18	640.	501.10	-202.60	-49.30	-398.30
19	780.	205.70	-109.10	13.70	-158.50

Table II

Kr ions

fit parameters A, B, C, D, E, F (units: 1e-16 cm^2 eV)
for evaluating ISEA ionisation cross sections and rates
according to, respectively, formulae 2 and 6
Z spectroscopic notations and IEA (eV) ISEA edges

Z	IEA	A	B	C	D	E	F
16	1640.	0.50	-1.70	0.	0.	0.	0.60
17	1650.	0.40	45.90	-82.60	45.70	0.	-1.50
18	1650.	0.50	3.50	-17.50	12.90	0.	0.40
19	1580.	0.50	-0.10	7.60	-22.60	15.40	-0.30

Table III

Mo ions

fit parameters A, B, C, D (units: 1e-14 cm^2 eV^2)
for evaluating DI ionisation cross sections and rates
according to, respectively, formulae 1 and 3
Z spectroscopic notations and I (eV) ionisation potentials

Z	I	A	B	C	D
1	7.1	-89.30	21.00	34.00	59.10
2	13.6	-70.00	30.90	29.20	39.50
3	26.	0.30	-5.20	36.80	2.70
4	40.	35.70	-118.60	84.20	7.60
5	54.	165.90	-137.50	32.10	-88.90
6	68.5	315.80	-236.90	20.50	-213.30
7	80.	-60.70	57.40	22.50	61.40
8	115.	-24.40	12.10	27.80	20.70
9	140.	-253.90	140.50	53.70	217.80
42	24600.	-50.42	13.14	17.92	36.96

Table IV

Ionisation Potentials for highly ionisad ions (eV)

isosequences	Kr ions	Mo ions
Ne-like	2953	3990
F-like	3056	4191
O-like	3203	4392
N-like	3381	4593
C-like	3555	4902
B-like	3712	5110
Be-like	3912	5407
Li-like	4105	5585
He-like	17292	23120
H-like	17931	24600

Table V

Kr ions

C and E coefficients for evaluating ionisation rates
of Kr I - XXXVI according to formula 9
fits of the tabulated data of Ref. [21]

Z	C1	C2	C3	C4	C5
1	1.406e+04	1.417e+05	2.091e+05	3.762e+05	-1.247e+05
2	1.546e+04	3.281e+04	1.002e+05	1.075e+05	
3	1.868e+04	5.009e+04	4.966e+04		
4	1.306e+04	2.714e+04	2.372e+04		
5	7.316e+03	1.083e+04	1.234e+04		
6	5.979e+03	2.458e+04	-9.476e+03	3.238e+04	5.834e+04
7	8.811e+03	2.377e+04	5.288e+04	-1.707e+03	
8	9.250e+03	2.346e+04	5.640e+04		
9	5.847e+03	2.109e+04	1.301e+04	3.524e+04	
10	5.967e+03	1.769e+04	2.932e+04		
11	5.644e+03	1.432e+04	2.433e+04		
12	4.571e+03	1.180e+04	1.886e+04		
13	3.941e+03	9.655e+03	1.492e+04		
14	3.570e+03	7.958e+03	1.142e+04		
15	2.663e+03	6.650e+03	9.209e+03		
16	2.281e+03	5.708e+03	7.076e+03		
17	1.649e+03	4.844e+03	5.704e+03		
18	1.279e+03	4.318e+03	4.477e+03		
19	9.871e+02	3.710e+03	3.095e+03		
20	8.580e+02	3.288e+03	2.444e+03		
21	6.411e+02	2.496e+03	1.241e+03		
22	5.811e+02	2.462e+03	1.619e+03		
23	4.583e+02	2.210e+03			
24	3.531e+02	1.710e+03			
25	2.294e+02	9.118e+02			
26	2.788e+02	9.747e+02	1.294e+03		
27	1.585e+02	4.708e+02	8.353e+02		
28	1.322e+02	4.041e+02	6.813e+02		
29	1.089e+02	3.269e+02	5.477e+02		
30	8.753e+01	2.642e+02	4.246e+02		
31	6.575e+01	1.798e+02	3.514e+02		
32	4.870e+01	1.357e+02	2.219e+02		
33	2.971e+01	1.013e+02	1.629e+02		
34	1.589e+01	4.924e+01	1.209e+02		
35	2.086e+00	1.146e+01	3.672e+01		
36	1.367e+00	9.615e+00	3.939e+01		

Z	E1	E2	E3	E4	E5
1	15.58	22.95	50.83	830.27	610.63
2	26.55	33.61	66.02	343.63	
3	41.07	72.86	549.98		
4	54.51	94.83	644.30		
5	69.87	118.57	868.54		
6	87.51	158.67	246.07	427.93	2077.08
7	126.49	237.26	1424.30	416.58	
8	136.37	262.98	1782.96		
9	260.14	445.85	1266.07	2878.08	
10	301.07	517.88	2012.08		
11	341.36	591.72	2717.66		
12	389.64	678.71	3113.23		
13	438.03	766.41	3450.50		
14	483.68	875.78	4003.39		
15	537.92	965.62	4332.71		
16	589.93	1096.03	4887.20		
17	648.72	1210.93	5506.10		
18	712.87	1381.41	6719.05		
19	883.88	1663.24	7974.53		
20	947.85	1797.41	9802.75		
21	1080.50	1749.15	4742.56		
22	1076.40	1953.53	12336.39		
23	1142.83	2036.01			
24	1226.66	2022.62			
25	1322.52	2069.08			
26	1490.83	2474.87	12643.79		
27	3151.50	4376.41	10683.44		
28	3307.08	4642.69	11589.77		
29	3480.12	4893.65	12244.30		
30	3651.37	5192.76	13260.98		
31	3835.22	5301.31	13917.00		
32	4037.05	5829.10	14757.38		
33	4247.48	6543.01	22430.62		
34	4417.73	6797.18	25679.19		
35	17811.50	21181.29	45508.69		
36	18562.84	24656.75	113860.55		

Table VI

Mo ions

C and E coefficients for evaluating ionisation rates
of Mo VII - XIV according to formula 9
using theoretical data from Refs [52, 53, 57, 58]

Z	C1	C2	C3	C4
7	7.938e+03	2.851e+04	4.671e+04	
8	5.865e+03	2.457e+04	4.140e+04	
9	4.544e+03	2.085e+04	3.544e+04	
10	3.928e+03	1.795e+04	3.069e+04	
11	4.172e+03	1.574e+04	2.699e+04	
12	4.901e+03	1.431e+04	2.398e+04	
13	9.140e+02	1.268e+04	1.860e+04	2.903e+04
14	1.947e+03	1.034e+04	1.720e+04	1.630e+04

Z	E1	E2	E3	E4
7	153.57	320.69	1158.93	
8	177.50	349.21	1259.32	
9	201.29	368.06	1290.63	
10	227.97	387.75	1320.88	
11	256.93	413.14	1374.29	
12	283.16	447.68	1476.27	
13	260.80	370.34	909.19	3727.01
14	302.48	411.73	1041.98	4118.62

Table VII

Mo ions

C and E coefficients for evaluating theoretical ionisation rate coefficients
of Mo XV - XXXIII according to formula 9. Used are C and E values for DI from Ref. [6]
(first two coefficients) and for ISEA from Ref. [60] (third and forth coefficients)

Z	C1	C2	C3	C4
15	1.511e+04	1.721e+04		
16	1.203e+04	1.434e+04		
17	9.637e+03	1.197e+04		
18	7.743e+03	1.001e+04		
19	8.368e+03	6.091e+03		
20	5.028e+03	6.987e+03		
21	4.052e+03	5.815e+03		
22	3.262e+03	4.819e+03		
23	2.616e+03	3.966e+03		
24	2.099e+03	3.232e+03	9.343e+02	2.509e+02
25	2.635e+03	1.629e+03	9.228e+02	9.827e+01
26	2.562e+03	1.107e+03	4.877e+02	6.365e+02
27	2.024e+03	8.507e+02	4.800e+02	6.265e+02
28	1.556e+03	6.355e+02	4.724e+02	6.166e+02
29	1.149e+03	4.561e+02	4.649e+02	6.068e+02
30	1.229e+03	3.108e+02	4.576e+02	5.972e+02
31	9.614e+02	1.814e+02	3.630e+02	5.231e+02
32	7.391e+02	8.550e+01	2.927e+02	4.200e+02
33	5.770e+02			

Z	E1	E2	E3	E4
15	769.00	2471.90		
16	829.10	2558.40		
17	891.20	2649.70		
18	954.67	2741.10		
19	2833.10	1019.90		
20	1087.50	2930.40		
21	1157.60	3029.70		
22	1230.20	3135.70		
23	1306.50	3247.30		
24	1388.50	3372.90	3362.30	1187.70
25	3509.20	1460.80	3209.10	1417.70
26	2685.00	1456.30	4719.40	2554.90
27	3784.40	1521.80	4719.40	2554.90
28	3890.90	1590.70	4719.50	2554.90
29	4017.60	1666.30	4719.40	2554.90
30	4189.90	1750.40	4719.50	2554.90
31	4531.70	1844.00	4959.70	2558.30
32	4936.30	1917.40	4893.40	2591.70
33	5712.70			

Table VIII

Kr ions

fit parameters (a, b, T0, T1) for the radiative recombination rates
of recombined Kr I - XXXVI according to formula 10

Z	A	b	T0	T1
1	1.674e-13	-0.3559	1.781e+00	1.488e+04
2	6.395e-13	-0.3246	3.271e+00	3.093e+03
3	1.521e-12	-0.2298	3.924e+00	2.575e+03
4	3.989e-12	0.1053	2.270e+00	7.712e+02
5	8.620e-12	0.4060	1.242e+00	3.731e+02
6	9.301e-12	0.4377	2.847e+00	4.202e+02
7	1.664e-11	0.5213	1.355e+00	5.051e+02

8	1.305e-11	0.5616	3.062e+00	4.823e+02
9	5.479e-11	0.1774	1.663e+00	8.708e+02
10	8.928e-11	0.3449	9.961e-01	7.278e+02
11	8.668e-11	0.1343	1.995e+00	2.004e+03
12	8.857e-11	0.1941	2.337e+00	2.151e+03
13	1.158e-10	0.4692	1.437e+00	9.265e+02
14	2.686e-10	0.4730	5.611e-01	1.297e+03
15	2.997e-10	0.4312	6.742e-01	1.881e+03
16	3.532e-10	0.5653	4.977e-01	1.295e+03
17	2.464e-10	0.5540	1.083e+00	1.497e+03
18	2.677e-10	0.5552	1.181e+00	1.739e+03
19	2.215e-10	0.5336	1.974e+00	2.194e+03
20	3.457e-10	0.5665	1.157e+00	2.352e+03
21	3.672e-10	0.5785	1.239e+00	2.511e+03
22	4.016e-10	0.5913	1.256e+00	2.687e+03
23	3.472e-10	0.5868	1.870e+00	2.947e+03
24	6.909e-10	0.6194	7.191e-01	3.143e+03
25	4.936E-10	0.5469	1.637E+00	1.254E+04
26	3.051e-10	0.4446	4.565e+00	2.180e+04
27	6.842e-10	0.5709	1.283e+00	1.440e+04
28	1.033e-09	0.6234	7.189e-01	1.221e+04
29	1.497E-09	0.6596	4.302E-01	1.100E+04
30	2.338E-09	0.6908	2.267E-01	1.089E+04
31	3.422E-09	0.7122	1.321E-01	9.539E+03
32	4.645e-09	0.7261	8.773e-02	9.333e+03
33	1.674e-09	0.6723	5.801e-01	1.530e+04
34	6.380e-10	0.5851	3.745e+00	2.706e+04
35	1.245e-09	0.6716	1.380e+00	6.604e+04
36	3.140e-09	0.7485	3.048e-01	7.809e+04

Mo ions

fit parameters (a, b, T0, T1) for the radiative recombination rates
of recombined Mo I - XLII according to formula 10

Z	A	b	T0	T1
1	1.957e-13	-0.5291	1.463e+00	1.338e+04
2	6.240e-13	-0.5466	3.553e+00	1.030e+04
3	1.471e-12	-0.4586	4.435e+00	2.306e+04
4	2.917e-12	-0.3003	4.389e+00	5.209e+03
5	4.284e-12	-0.3264	5.733e+00	2.246e+04
6	5.520e-12	-0.2934	7.212e+00	3.042e+04
7	1.296e-11	0.4939	1.895e+00	5.057e+02
8	1.231e-11	0.3650	3.673e+00	9.595e+02
9	1.719e-11	0.2832	3.775e+00	1.726e+03
10	2.119e-11	0.6012	2.857e+00	6.756e+02
11	3.238e-11	0.3075	3.078e+00	2.695e+03
12	7.906e-11	0.7260	5.463e-01	7.453e+02
13	1.018e-10	0.7960	4.150e-01	7.186e+02
14	7.954e-11	0.8113	8.177e-01	7.658e+02
15	1.307e-10	0.1730	2.878e+00	3.288e+03
16	4.548e-10	0.3799	5.181e-01	1.864e+03
17	7.165e-10	0.5847	1.997e-01	1.085e+03
18	5.057e-10	0.5883	4.042e-01	1.259e+03
19	4.193e-10	0.5523	7.132e-01	1.612e+03
20	3.633e-10	0.5573	1.039e+00	1.844e+03
21	4.197e-10	0.5710	9.768e-01	2.031e+03
22	4.314e-10	0.5782	1.097e+00	2.238e+03
23	3.978e-10	0.5782	1.463e+00	2.485e+03
24	4.950e-10	0.5787	1.230e+00	2.928e+03
25	5.303e-10	0.5794	1.286e+00	3.416e+03
26	5.297e-10	0.5856	1.474e+00	3.678e+03
27	7.549e-10	0.6109	9.434e-01	3.778e+03
28	8.507e-10	0.6237	8.760e-01	3.967e+03
29	8.531e-10	0.6280	9.864e-01	4.287e+03
30	9.489e-10	0.6387	9.420e-01	4.489e+03
31	6.295E-10	0.5525	2.371E+00	1.591E+04
32	3.541e-10	0.4350	7.654e+00	2.873e+04
33	8.282e-10	0.5708	1.938e+00	1.890e+04
34	1.256e-09	0.6232	1.051e+00	1.622e+04
35	1.748E-09	0.6593	6.572E-01	1.469E+04
36	2.791E-09	0.6893	3.275E-01	1.364E+04
37	4.461E-09	0.7147	1.615E-01	1.276E+04
38	6.974e-09	0.7318	8.292e-02	1.239e+04
39	1.926e-09	0.6717	8.602e-01	2.075e+04
40	8.161e-10	0.5972	4.379e+00	3.493e+04
41	1.536e-09	0.6764	1.734e+00	8.686e+04
42	3.583e-09	0.7474	4.316e-01	1.064e+05

Table IX

Kr ions

C and E coefficients for dielectronic recombination rates
of recombined Kr I - XXXV according to formula 11

Z	C1	C2	C3	C4	C5	C6	C7
1	3.506e-09						
2	9.914e-09						
3	1.656e-08	6.930e-10					
4	1.870e-08	1.821e-09					
5	1.736e-08	3.636e-09					
6	7.855e-09	5.456e-09					
7	5.545e-09	-4.990e-12	7.566e-09				
8	2.555e-09	2.518e-08	7.594e-09				
9	5.936e-08	5.297e-08					
10	7.242e-08	1.203e-07					
11	2.751e-07						
12	3.957e-07						
13	4.865e-07						
14	5.813e-07						
15	5.708e-07	1.394e-07					
16	6.708e-07	1.548e-07					
17	8.893e-07						
18	1.139e-06	4.722e-07					
19	1.006e-06	4.371e-07					
20	9.836e-07	4.403e-07					
21	3.592e-08	8.306e-07	6.246e-07				
22	2.279e-07	6.358e-07					
23	3.708e-07	2.883e-07	5.419e-08				
24	1.599e-07	2.133e-06	2.597e-07				
25	1.326e-09	4.784e-08	1.122e-07	1.566e-07	4.699e-07	1.978e-06	1.057e-08
26	2.457e-09	5.237e-07	2.397e-06	4.766e-07	-7.295e-08		
27	4.556e-10	2.475e-09	1.219e-08	8.400e-08	1.283e-06	2.281e-06	
28	1.362e-09	1.190e-08	3.946e-08	1.355e-07	1.145e-06	2.250e-06	7.386e-08
29	3.025e-09	2.182e-08	6.246e-08	1.126e-07	7.100e-07	2.854e-06	
30	1.902e-09	3.019e-08	7.424e-08	1.457e-07	6.501e-07	1.902e-06	1.115e-08
31	2.431e-09	3.479e-08	9.920e-08	1.981e-07	7.350e-07	1.436e-06	
32	4.914e-09	1.920e-08	1.394e-07	1.890e-07	5.373e-07	5.373e-07	4.509e-07
33	3.820e-09	2.453e-08	9.744e-08	8.792e-08	6.338e-07	6.059e-07	2.560e-08
34	3.134e-07	5.537e-07	-1.075e-07				
35	2.142e-07	2.746e-07	-2.361e-09				

Z	E1	E2	E3	E4	E5	E6	E7
1	1.494e+00						
2	2.182e+00						
3	2.649e+00	6.478e+01					
4	2.713e+00	1.056e+01					
5	2.504e+00	1.612e+02					
6	1.970e+00	1.407e+01					
7	2.314e+00	5.340e+01	1.852e+01				
8	1.677e+01	1.568e+02	4.850e+01				
9	5.949e+01	9.735e+01					
10	7.118e+01	9.698e+01					
11	9.074e+01						
12	9.403e+01						
13	3.943e+01						
14	8.893e+01						
15	8.683e+01	1.419e+02					
16	8.494e+01	1.567e+02					
17	8.294e+01						
18	9.659e+01	2.415e+02					
19	9.943e+01	2.704e+02					
20	9.826e+01	2.673e+02					
21	4.760e+01	8.484e+01	2.590e+02				
22	5.336e+01	1.243e+02					
23	5.371e+01	1.572e+02	3.633e+03				
24	4.386e+01	1.331e+03	3.815e+02				
25	2.727e+00	9.651e+00	3.494e+01	7.749e+01	5.359e+02	1.430e+03	1.989e+04
26	4.440e+02	6.726e+02	1.324e+03	2.791e+03	6.394e+03		
27	1.366e+00	1.196e+01	3.538e+01	2.175e+02	8.541e+02	1.670e+03	
28	1.433e+00	1.013e+01	4.208e+01	2.059e+02	8.462e+02	1.636e+03	4.079e+03
29	2.291e+00	1.050e+01	3.995e+01	1.346e+02	6.349e+02	1.616e+03	
30	1.455e+00	1.196e+01	4.377e+01	1.585e+02	7.836e+02	1.758e+03	1.298e+05
31	1.289e+00	1.424e+01	5.099e+01	1.698e+02	8.962e+02	1.875e+03	
32	8.412e-01	1.296e+01	6.251e+01	2.746e+02	1.592e+03	1.593e+03	9.850e+03
33	4.343e+00	1.432e+01	6.952e+01	4.209e+02	1.685e+03	9.944e+03	3.166e+04
34	9.005e+03	1.209e+04	1.320e+04				
35	9.195e+03	1.226e+04	1.728e+04				

Mo ions

C and E coefficients for dielectronic recombination rates
of recombined Mo I - XLI according to formula 11

Z	C1	C2	C3	C4	C5	C6	C7
1	1.842e-10	1.299e-08					
2	6.827e-10	3.548e-08					
3	1.685e-09	7.231e-08					
4	2.200e-07						
5	3.475e-07						
6	5.083e-07	1.434e-07					
7	5.135e-07	2.591e-07					
8	4.845e-07	4.167e-07					
9	4.133e-07	6.207e-07					
10	3.006e-07	8.758e-07					
11	1.662e-07	1.145e-06					
12	2.910e-07	1.557e-06					
13	1.329e-07	2.247e-06					
14	8.782e-09	4.353e-07	7.870e-08				
15	1.011e-07	1.261e-06					
16	2.211e-07	1.427e-06					
17	4.202e-07	1.390e-06					
18	5.873e-07	1.471e-06					
19	6.349e-07	2.573e-07					
20	7.612e-07	2.746e-07					
21	9.267e-07	2.910e-07					
22	1.033e-06	3.112e-07					
23	1.302e-06	1.986e-07					
24	6.170e-07	3.531e-07	6.805e-07	8.802e-07	1.089e-06		
25	9.452e-07	4.169e-07	6.032e-07	1.048e-06	1.132e-06		
26	1.021e-06	4.827e-07	6.410e-07	3.965e-07	9.822e-07	9.393e-07	
27	9.905e-07	4.681e-07	5.664e-07	1.262e-06	1.740e-06		
28	8.892e-07	4.202e-07	4.813e-07	1.570e-06	2.176e-06		
29	7.255e-07	3.429e-07	3.857e-07	1.881e-06	1.791e-06		
30	5.060e-07	2.022e-07	2.360e-07	2.837e-06	1.805e-06		
31	1.005e-08	3.982e-08	2.430e-07	1.982e-07	8.056e-07	2.856e-06	2.192e-08
32	5.690e-09	8.272e-07	3.151e-06	6.676e-07	-9.136e-08		
33	1.153e-09	1.580e-08	2.174e-08	1.660e-07	1.898e-06	2.818e-06	
34	6.473e-09	2.474e-08	6.650e-08	2.358e-07	1.897e-06	2.618e-06	1.834e-08
35	2.229e-09	3.997e-08	1.037e-07	2.140e-07	1.310e-06	3.309e-06	
36	4.395e-08	3.210e-08	1.327e-07	2.290e-07	1.043e-06	2.331e-06	
37	6.494e-09	4.630e-08	1.508e-07	2.930e-07	8.848e-07	1.935e-06	
38	1.743e-08	6.540e-08	9.000e-08	2.225e-07	2.982e-07	1.310e-06	4.958e-07
39	3.162e-08	1.829e-08	1.008e-07	1.096e-07	5.437e-07	4.102e-07	6.058e-07
40	3.699e-07	4.037e-07	4.317e-08	1.645e-09			
41	2.221e-07	2.880e-07	1.038e-09				

Z	E1	E2	E3	E4	E5	E6	E7
1	1.494e+00	6.974e+00					
2	2.961e+00	7.895e+00					
3	4.877e+00	1.073e+01					
4	3.846e+01						
5	3.874e+01						
6	3.877e+01	2.635e+02					
7	3.999e+01	2.681e+02					
8	4.110e+01	2.717e+02					
9	4.207e+01	2.748e+02					
10	4.297e+01	2.781e+02					
11	4.382e+01	2.779e+02					
12	2.820e+01	2.841e+02					
13	2.714e+01	2.876e+02					
14	2.576e+01	2.474e+02	8.929e+01				
15	1.433e+02	3.047e+02					
16	1.388e+02	3.222e+02					
17	1.342e+02	3.410e+02					
18	1.318e+02	3.572e+02					
19	1.169e+02	2.100e+02					
20	1.116e+02	2.288e+02					
21	1.103e+02	2.486e+02					
22	1.068e+02	2.688e+02					
23	1.031e+02	6.946e+02					
24	5.729e+02	8.814e+01	5.721e+01	1.689e+03	2.491e+03		
25	4.186e+02	7.606e+01	6.122e+01	1.705e+03	2.624e+03		
26	4.404e+02	4.332e+01	4.428e+01	1.094e+03	2.394e+03	1.832e+03	
27	4.404e+02	4.332e+01	4.428e+01	1.340e+03	2.498e+03		
28	4.404e+02	4.332e+01	4.428e+01	1.339e+03	2.493e+03		
29	4.404e+02	4.332e+01	4.428e+01	1.339e+03	2.492e+03		
30	4.859e+02	3.687e+01	3.850e+01	2.458e+03	1.278e+03		
31	2.779e+00	1.107e+01	5.064e+01	1.167e+02	6.861e+02	1.959e+03	4.231e+04
32	5.965e+02	8.962e+02	1.809e+03	3.085e+03	1.015e+04		
33	1.163e+00	1.148e+01	7.714e+01	3.422e+02	1.173e+03	2.339e+03	
34	2.827e+00	1.099e+01	6.814e+01	3.038e+02	1.197e+03	2.415e+03	6.599e+04
35	1.252e+01	2.825e+01	6.793e+01	2.282e+02	9.856e+02	2.305e+03	
36	3.216e+00	1.173e+01	6.497e+01	2.246e+02	1.067e+03	2.462e+03	
37	1.749e+00	1.680e+01	6.539e+01	2.160e+02	1.059e+03	2.501e+03	
38	3.405e+00	1.154e+01	6.442e+01	1.636e+02	6.852e+02	2.335e+03	1.473e+04
39	2.937e+00	1.596e+01	7.245e+01	2.309e+02	1.544e+03	3.853e+03	1.573e+04
40	1.236e+04	1.580e+04	1.966e+04	7.924e+04			
41	1.256e+04	1.658e+04	3.589e+04				

Table X

fractional abundances of Kr ions (spectroscopic notations) as functions of Te (eV)

log10(Te)	1	2	3	4	5	6	7	8	9	10	11	12	13
0.00	1.0000												
0.10	0.9992	0.0008											
0.20	0.9907	0.0093											
0.30	0.9326	0.0673											
0.40	0.7128	0.2878	0.0003										
0.50	0.3594	0.6334	0.0073										
0.60	0.1273	0.8012	0.0711	0.0004									
0.70	0.0334	0.6386	0.3150	0.0130									
0.80	0.0054	0.2760	0.5796	0.1369	0.0020								
0.90	0.0005	0.0612	0.4423	0.4517	0.0438	0.0004							
1.00		0.0075	0.1577	0.5579	0.2584	0.0180	0.0004						
1.10		0.0005	0.0278	0.2850	0.4916	0.1715	0.0234	0.0002					
1.20			0.0021	0.0551	0.2897	0.3915	0.2435	0.0161	0.0019				
1.30			0.0001	0.0035	0.0479	0.2036	0.4571	0.1777	0.1099	0.0002			
1.40				0.0001	0.0019	0.0215	0.1451	0.2439	0.5805	0.0070			

1.50						0.0011	0.0194	0.1121	0.8126	0.0542	0.0005	
1.60							0.0024	0.0406	0.7407	0.2058	0.0103	0.0001
1.70							0.0003	0.0118	0.4652	0.4328	0.0860	0.0039
1.80								0.0023	0.1770	0.4655	0.2986	0.0539
1.90								0.0003	0.0369	0.2398	0.4232	0.2504
2.00									0.0039	0.0566	0.2424	0.3996
2.05									0.0010	0.0202	0.1296	0.3391
2.10									0.0002	0.0058	0.0546	0.2203
2.15										0.0014	0.0182	0.1104
2.20										0.0003	0.0049	0.0435
2.25											0.0011	0.0139
2.30											0.0002	0.0037
2.35												0.0008
2.40												0.0002
2.45												0.0005

log10(Te)	14	15	16	17	18	19	20	21	22	23	24	25
1.80	0.0001											
1.90	0.0039	0.0001										
2.00	0.0646	0.0085	0.0004									
2.05	0.1552	0.0368	0.0033	0.0001								
2.10	0.2656	0.1077	0.0171	0.0013								
2.15	0.3285	0.2196	0.0590	0.0080	0.0004							
2.20	0.3020	0.3213	0.1402	0.0327	0.0032	0.0001						
2.25	0.2135	0.3504	0.2404	0.0922	0.0159	0.0010						
2.30	0.1194	0.2939	0.3076	0.1877	0.0541	0.0057	0.0003					
2.35	0.0538	0.1940	0.3016	0.2840	0.1322	0.0226	0.0022					
2.40	0.0199	0.1029	0.2320	0.3278	0.2390	0.0645	0.0107	0.0007				
2.45	0.0062	0.0448	0.1436	0.2973	0.3303	0.1365	0.0363	0.0041	0.0003			
2.50	0.0016	0.0164	0.0732	0.2174	0.3590	0.2216	0.0915	0.0168	0.0020	0.0002		
2.55	0.0004	0.0051	0.0312	0.1382	0.3126	0.2819	0.1751	0.0510	0.0101	0.0020	0.0003	
2.60		0.0013	0.0110	0.0637	0.2179	0.2814	0.2565	0.1158	0.0361	0.0118	0.0033	0.0010
2.65		0.0003	0.0031	0.0246	0.1175	0.2132	0.2768	0.1904	0.0914	0.0473	0.0217	0.0097
2.70			0.0006	0.0067	0.0442	0.1109	0.2040	0.2062	0.1483	0.1187	0.0861	0.0563
2.75				0.0011	0.0102	0.0348	0.0885	0.1295	0.1362	0.1641	0.1833	0.1682
2.80				0.0001	0.0015	0.0069	0.0240	0.0498	0.0748	0.1323	0.2212	0.2765
2.85					0.0002	0.0011	0.0051	0.0146	0.0306	0.0777	0.1895	0.3140
2.90						0.0002	0.0010	0.0038	0.0110	0.0393	0.1365	0.2932
2.95							0.0002	0.0010	0.0038	0.0186	0.0897	0.2452
3.00								0.0003	0.0013	0.0085	0.0559	0.1910
3.05									0.0004	0.0038	0.0336	0.1415
3.10										0.0017	0.0196	0.1005
3.15										0.0007	0.0111	0.0685
3.20										0.0003	0.0060	0.0446
3.25											0.0031	0.0273
3.30											0.0015	0.0154
3.40											0.0002	0.0034
3.50												0.0004

log10(Te)	26	27	28	29	30	31	32	33	34	35	36	37
2.65	0.0016	0.0003										
2.70	0.0139	0.0039										
2.75	0.0605	0.0231	0.0002									
2.80	0.1402	0.0717	0.0010									
2.85	0.2175	0.1461	0.0038									
2.90	0.2701	0.2345	0.0101	0.0003								
2.95	0.2936	0.3245	0.0225	0.0010								
3.00	0.2916	0.4047	0.0435	0.0031								
3.05	0.2706	0.4662	0.0750	0.0002	0.0006							
3.10	0.2374	0.5018	0.1176	0.0191	0.0020	0.0002						
3.15	0.1973	0.5070	0.1686	0.0396	0.0062	0.0008						
3.20	0.1548	0.4793	0.2213	0.0735	0.0164	0.0032	0.0004					
3.25	0.1134	0.4199	0.2642	0.1211	0.0379	0.0105	0.0020	0.0003				
3.30	0.0760	0.3346	0.2824	0.1756	0.0754	0.0290	0.0078	0.0018	0.0003			
3.40	0.0231	0.1421	0.2076	0.2272	0.1745	0.1224	0.0606	0.0273	0.0090	0.0025		
3.50	0.0033	0.0278	0.0674	0.1241	0.1621	0.1955	0.1686	0.1347	0.0781	0.0380		
3.60	0.0002	0.0024	0.0094	0.0279	0.0597	0.1185	0.1705	0.2277	0.2167	0.1665	0.0005	
3.70			0.0008	0.0038	0.0130	0.0409	0.0948	0.2025	0.2994	0.3416	0.0030	
3.80				0.0005	0.0024	0.0115	0.0416	0.1366	0.3024	0.4940	0.0110	
3.90					0.0004	0.0038	0.0167	0.0815	0.2631	0.6045	0.0300	0.0008
4.00						0.0008	0.0064	0.0452	0.2089	0.6684	0.0668	0.0035
4.10							0.0024	0.0237	0.1540	0.6807	0.1270	0.0119
4.20							0.0009	0.0118	0.1060	0.6402	0.2089	0.0321
4.30								0.0056	0.0683	0.5561	0.2985	0.0711

Table XI

fractional abundances of Mo ions (spectroscopic notations) as functions of Te (eV)

log10(Te)	1	2	3	4	5	6	7	8	9	10	11	
0.00	0.5260	0.4739	0.0001									
0.10	0.2431	0.7556	0.0013									
0.20	0.1182	0.8709	0.0109									
0.30	0.0624	0.8855	0.0521									
0.40	0.0321	0.7965	0.1705	0.0010								
0.50	0.0142	0.5894	0.3020	0.0126	0.0018							
0.60	0.0046	0.3067	0.5245	0.0751	0.0883	0.0089						
0.70	0.0007	0.0751	0.3041	0.1505	0.4436	0.0260						
0.80		0.0102	0.0895	0.1283	0.6522	0.1186	0.0011					
0.90		0.0012	0.0210	0.0760	0.6123	0.2794	0.01					
1.00			0.0045	0.0364	0.4510	0.4549	0.0526	0.0005				
1.10			0.0009	0.0143	0.2671	0.5424	0.1698	0.0055				
1.20				0.0046	0.1264	0.4794	0.3549	0.0344	0.0002			
1.30				0.0012	0.0479	0.3195	0.5013	0.1273	0.0028			
1.40				0.0003	0.0147	0.1647	0.5012	0.2972	0.0214	0.0005		
1.50					0.0037	0.0666	0.3664	0.4619	0.0935	0.0077	0.0001	
1.60					0.0007	0.0207	0.1944	0.4821	0.2401	0.0587	0.0031	
1.70						0.0045	0.0690	0.3152	0.3462	0.2159	0.0406	
1.80						0.0006	0.0133	0.1053	0.2324	0.3253	0.1812	
1.90							0.0007	0.0098	0.0402	0.1128	0.1590	
2.00								0.0002	0.0014	0.0072	0.0223	
2.05									0.0002	0.0015	0.0066	
2.10										0.0003	0.0019	
2.15											0.0006	

log10(Te)	12	13	14	15	16	17	18	19	20	21	22
1.60	0.0002										
1.70	0.0079	0.0004									
1.80	0.1094	0.0226	0.0065	0.0036							
1.90	0.2412	0.1460	0.1147	0.1727	0.0027						
2.00	0.0712	0.1030	0.1713	0.5768	0.0454	0.0012					
2.05	0.0290	0.0609	0.1377	0.6565	0.1017	0.0057					
2.10	0.0113	0.0332	0.0988	0.6485	0.1846	0.0204	0.0009				
2.15	0.0042	0.0169	0.0645	0.5699	0.2812	0.0576	0.0049				
2.20	0.0015	0.0079	0.0380	0.4423	0.3597	0.1287	0.0204	0.0014			
2.25	0.0005	0.0033	0.0196	0.2973	0.3812	0.2261	0.0630	0.0083	0.0007		
2.30		0.0012	0.0087	0.1691	0.3290	0.3090	0.1439	0.0332	0.0053	0.0004	
2.35		0.0004	0.0032	0.0796	0.2271	0.3246	0.2412	0.0924	0.0270	0.0041	0.0003
2.40			0.0010	0.0301	0.1225	0.2574	0.2928	0.1783	0.0898	0.0244	0.0034
2.45				0.0088	0.0498	0.1493	0.2511	0.2333	0.1934	0.0890	0.0218
2.50				0.0019	0.0148	0.0616	0.1486	0.2036	0.2667	0.1993	0.0814
2.55				0.0003	0.0032	0.0182	0.0615	0.1206	0.2408	0.2889	0.1837
2.60					0.0005	0.0040	0.0186	0.0509	0.1503	0.2647	0.2670
2.65						0.0007	0.0043	0.0160	0.0680	0.1755	0.2648
2.70							0.0008	0.0038	0.0230	0.0848	0.1862
2.75							0.0001	0.0007	0.0059	0.0308	0.0960
2.80									0.0012	0.0087	0.0377
2.85									0.0002	0.0019	0.0116
2.90										0.0004	0.0028
2.95											0.0006

log10(Te)	23	24	25	26	27	28	29	30	31	32	33
2.40	0.0003										
2.45	0.0030	0.0002									
2.50	0.0193	0.0026	0.0003								
2.55	0.0713	0.0162	0.0029	0.0002							
2.60	0.1635	0.0603	0.0174	0.0025	0.0002						
2.65	0.2472	0.1424	0.0640	0.0146	0.0022	0.0002					
2.70	0.2574	0.2239	0.1515	0.0534	0.0129	0.0019	0.0002				
2.75	0.1917	0.2450	0.2419	0.1271	0.0477	0.0110	0.0019	0.0003			
2.80	0.1063	0.1949	0.2730	0.2080	0.1173	0.0399	0.0103	0.0021	0.0004		
2.85	0.0454	0.1170	0.2269	0.2443	0.2017	0.0989	0.0371	0.0112	0.0031	0.0006	
2.90	0.0152	0.0540	0.1422	0.2118	0.2490	0.1722	0.0915	0.0394	0.0158	0.0045	0.0012
2.95	0.0040	0.0193	0.0677	0.1369	0.2238	0.2137	0.1573	0.0945	0.0529	0.0214	0.0078
3.00	0.0008	0.0053	0.0245	0.0661	0.1468	0.1903	0.1903	0.1561	0.1190	0.0673	0.0328
3.05		0.0012	0.0069	0.0242	0.0717	0.1241	0.1656	0.1822	0.1857	0.1434	0.0920
3.10			0.0016	0.0071	0.0276	0.0628	0.1101	0.1598	0.2141	0.2218	0.1848
3.15			0.0003	0.0018	0.0091	0.0268	0.0607	0.1145	0.1985	0.2714	0.2909
3.20				0.0004	0.0027	0.0103	0.0298	0.0720	0.1595	0.2836	0.3868
3.25					0.0008	0.0038	0.0137	0.0418	0.1167	0.2661	0.4575
3.30						0.0013	0.0060	0.0230	0.0799	0.2308	0.4956
3.40							0.0011	0.0061	0.0322	0.1443	0.4705
3.50								0.0014	0.0105	0.0705	0.3378
3.60									0.0025	0.0243	0.1664
3.70									0.0003	0.0047	0.0446
3.80										0.0004	0.0055
3.90											0.0004

log10(Te)	34	35	36	37	38	39	40	41	42	43
3.00	0.0006									
3.05	0.0029									
3.10	0.0098	0.0002								
3.15	0.0249	0.0010								
3.20	0.0513	0.0032								
3.25	0.0905	0.0086	0.0005							
3.30	0.1416	0.0196	0.0018	0.0001						
3.40	0.2576	0.0717	0.0138	0.0023	0.0003					
3.50	0.3233	0.1687	0.0620	0.0199	0.0045	0.0009	0.0002			
3.60	0.2591	0.2382	0.1569	0.0919	0.0393	0.0153	0.0048	0.0011		
3.70	0.1068	0.1650	0.1849	0.1864	0.1396	0.0956	0.0520	0.02		
3.80	0.0193	0.0402	0.0882	0.1464	0.1828	0.2081	0.1860	0.1141	0.0009	
3.90	0.0020	0.0077	0.0222	0.0585	0.1171	0.2119	0.2971	0.2770	0.0062	
4.00	0.0002	0.0010	0.0043	0.0173	0.0538	0.1495	0.3171	0.4339	0.0228	
4.10		0.0001	0.0008	0.0046	0.0216	0.0892	0.2784	0.5449	0.0596	0.0009
4.20			0.0001	0.0012	0.0080	0.0483	0.2173	0.5975	0.1240	0.0036
4.30				0.0003	0.0028	0.0244	0.1554	0.5916	0.2141	0.0114